

## A Near-Global Climatology of Single-Layer and Overlapped Clouds and Their Optical Properties Retrieved from *Terra/MODIS* Data Using a New Algorithm

FU-LUNG CHANG

*Earth System Science Interdisciplinary Center, University of Maryland, College Park, College Park, Maryland*

ZHANQING LI

*Earth System Science Interdisciplinary Center, and Department of Atmospheric and Oceanic Science, University of Maryland, College Park, College Park, Maryland*

(Manuscript received 8 June 2004, in final form 10 May 2005)

### ABSTRACT

Cloud overlapping has been a major issue in climate studies owing to a lack of reliable information available over both oceans and land. This study presents the first near-global retrieval and analysis of single-layer and overlapped cloud vertical structures and their optical properties retrieved by applying a new method to the Moderate Resolution Imaging Spectroradiometer (MODIS) data. Taking full advantage of the MODIS multiple channels, the method can differentiate cirrus overlapping lower water clouds from single-layer clouds. Based on newly retrieved cloud products using daytime *Terra/MODIS* 5-km overcast measurements sampled in January, April, July, and October 2001, global statistics of the frequency of occurrence, cloud-top pressure/temperature ( $P_c/T_c$ ), visible optical depth ( $\tau_{VIS}$ ), and infrared emissivity ( $\epsilon$ ) are presented and discussed. Of all overcast scenes identified over land (ocean), the MODIS data show 61% (52%) high clouds ( $P_c < 500$  hPa), 39% (48%) lower clouds ( $P_c > 500$  hPa), and an extremely low occurrence (<4%) of  $P_c$  between 500 and 600 hPa. A distinct bimodal distribution of  $P_c$  is found and peaks at  $\sim 275$  and  $\sim 725$  hPa for high and low clouds, thus leaving a minimum in cloud in the middle troposphere. Out of the 61% (52%) of high clouds identified by MODIS, retrievals reveal that 41% (35%) are thin cirrus clouds ( $\epsilon < 0.85$  and  $P_c < 500$  hPa) and the remaining 20% (17%) are thick high clouds ( $\epsilon \geq 0.85$ ). Out of the 41% (35%) of thin cirrus, 29% (27%) are found to overlap with lower water clouds and 12% (8%) are single-layer cirrus. Total low-cloud amount (single-layer plus overlapped) out of all overcast scenes is thus 68% (39% + 29%) over land and 75% (48% + 27%) over ocean, which is greater than the cloud amounts reported by the MODIS and the International Satellite Cloud Climatology Project (ISCCP). Both retrieved overlapping and nonoverlapping cirrus clouds show similar mean  $\tau_{VIS}$  of  $\sim 1.5$  and mean  $\epsilon$  of  $\sim 0.5$ . The optical properties of single-layer cirrus and single-layer water clouds agree well with the MODIS standard retrievals. Because the MODIS retrievals do not differentiate between cirrus and lower water clouds in overlap situations, large discrepancies are found for emissivity, cloud-top height, and optical depth for high cirrus overlapping lower water clouds.

### 1. Introduction

Clouds influence the earth's radiation budget by 1) reflecting solar radiation back to space and 2) trapping longwave radiation in the earth-atmosphere system. Unlike many low clouds that have a cooling effect on solar radiation through reflection, high thin cirrus

clouds reflect only a small amount of solar radiation and prevent a large quantity of longwave radiation from leaving the earth-atmosphere system (Liou 1986). They usually exert a net radiative heating on the system rather than cooling, as other types of clouds do (Ramaswamy and Ramanathan 1989; Hartmann et al. 1992). The horizontal coverage of cirrus clouds and their vertical distribution in the upper atmosphere are also linked to atmospheric circulation and the water cycle (Stephens et al. 1990).

To gain a better understanding of the earth's radiation budget and to improve weather and climate modeling, it is essential to accurately identify these cirrus

Corresponding author address: Dr. F.-L. Chang, Earth System Science Interdisciplinary Center, Computer and Space Sciences Bldg., University of Maryland, College Park, Rm. 2207, College Park, MD 20742.  
E-mail: fchang@essic.umd.edu

clouds and determine their optical properties. Surface observations from ships rarely report cirrus clouds existing alone (Warren et al. 1985). When low clouds are present, it is almost impossible to observe cirrus cloud height and optical properties. Indirect inference from global radiosonde water vapor profile data also indicates that  $\sim 40\%$  of all cloud observations consist of multilayer clouds (Poore et al. 1995; Wang et al. 2000). Extremely low water vapor amounts in the upper atmosphere can incur large uncertainties in determining cirrus clouds. Active sensors like airborne lidar (Sassen 1991; Platt et al. 1994; Clothiaux et al. 2000) and surface-based radar (Mace and Benson-Troth 2002) can more effectively determine multilayer clouds, but are limited to a few ground locations.

Satellite remote sensing is the only means of observing cloud and other climate variables on a global scale, an objective addressed by the International Satellite Cloud Climatology Project (ISCCP) (Rossow and Schiffer 1991, 1999). However, there is a dearth of information concerning the global climatology of cloud vertical structure and cirrus cloud properties. This is because the commonly used visible (VIS) and infrared (IR) measurements made by weather satellites ( $\sim 4\text{--}8$  km at nadir resolution) are often overwhelmed by thicker/lower water clouds. For example, ISCCP implements the bispectral method, which uses a VIS channel ( $\sim 0.6 \mu\text{m}$ ) for the cloud optical depth retrieval and an IR channel ( $\sim 11 \mu\text{m}$ ) for the cloud-top height retrieval. The ISCCP data are much more reliable in depicting horizontal distributions of column-integrated cloud amounts and optical depths than in probing the vertical distribution of cloud layers, especially when thin cirrus clouds are encountered. Thin cirrus clouds have faint signals that are difficult to detect in both the VIS and IR channels. When cirrus overlaps thicker low cloud, the  $11\text{-}\mu\text{m}$  brightness temperature represents the bulk emission from the much warmer low cloud. On the other hand, the very cold temperature of cirrus cloud can lower the total thermal radiance so that the inferred cloud-top temperature may be significantly colder than the real temperature of the lower cloud but warmer than the real temperature of the higher cirrus cloud. As such an intermediately warm midlevel cloud would be inferred. This leads to the general underestimation of high cloud amounts in ISCCP data (Jin et al. 1996) and the problematic retrieval of optical depth for either of the overlapped cirrus or lower water clouds. Considering the frequent occurrence of overlapped clouds, caution is warranted when using the *layered*-cloud statistics as reported in the ISCCP (Rossow and Schiffer 1991, 1999; Jin et al. 1996) or any other cloud data retrieved

from VIS-IR radiances for model validation and comparison (Zhang et al. 2005).

Another cirrus cloud climatology was inferred from the High-resolution Infrared Radiometer Sounder (HIRS) data on board the National Oceanic and Atmospheric Administration (NOAA) polar-orbiting satellite (Wylie et al. 1994; Wylie and Menzel 1999). The HIRS analyses employed several infrared channels near the  $15\text{-}\mu\text{m}$   $\text{CO}_2$  absorbing band and used a technique known as the  $\text{CO}_2$ -slicing method to determine cirrus cloud-top altitude. Effective cirrus cloud amounts were estimated from the  $11\text{-}\mu\text{m}$  channel. It was reported that high-level transmissive clouds covered more than 30% of the globe and more than 50% of the tropical regions on a monthly mean basis. While the HIRS is sensitive in detecting cirrus clouds, it does not detect low clouds obscured by the cirrus clouds. Another major uncertainty is associated with the large field of view of the HIRS pixel ( $\sim 20$  km at nadir resolution).

A few experimental techniques for cloud overlap detection have been proposed for application to the Moderate Resolution Imaging Spectroradiometer (MODIS) Airborne Simulator (MAS) data (Baum and Spinhirne 2000), the Advanced Very High Resolution Radiometer (AVHRR) data (Baum et al. 1995, 1997; Ou et al. 1996), and the National Polar-orbiting Operational Environmental Satellite System (NPOESS) data (Pavolonis and Heidinger 2004). These techniques are primarily concerned with the identification of multilayer scenes rather than the determination of cloud optical properties for the differentiated layers. Other satellite techniques have been proposed for retrieving multilayer clouds over ocean environments using a combination of microwave, visible, and infrared imager data (Sheu et al. 1997; Lin et al. 1998; Ho et al. 2003). The large variability of surface emissivity over land limits their application over oceans. Only the radiative effective heights of optically thick clouds can be determined from these techniques.

The MODIS provides unprecedented measurements at many more spectral channels and at high spatial resolution (King et al. 2003). The MODIS standard product provides much better information on cirrus cloud-top heights using the  $\text{CO}_2$ -slicing method (Platnick et al. 2003). Because the MODIS retrieval method assumes a single-layer cloud it does not provide information concerning the presence of a lower cloud layer beneath the cirrus cloud layer so no effort is made to separate the total column-integrated cloud optical depth in terms of high and low clouds. In this study, we apply a new retrieval method developed by Chang and Li (2005) to 1 yr of MODIS data in order to obtain gross but

distinct climatologies of 1) the frequency distributions of cirrus-overlapping-water clouds and single-layer clouds and 2) their corresponding cloud-top altitudes, optical depths, and cirrus cloud emissivities. These are retrieved from the *Terra*/MODIS level-1B 1-km VIS and IR radiance data, together with the MODIS level-2 cloud mask (Ackerman et al. 1998) and cloud-top property products (Menzel et al. 2002; Platnick et al. 2003). We classify clouds into different categories based on cloud-top pressure ( $P_c$ ), visible optical depth ( $\tau_{VIS}$ ), 11- $\mu\text{m}$ -high cloud emissivity ( $\epsilon_{hc}$ ), and overlapping information. The frequency of occurrence and retrieved optical properties for each cloud category are analyzed and compared for January, April, July, and October 2001.

Section 2 describes the MODIS data and the retrieval method. Section 3 presents the determination of different cloud categories and analyses of near-global cloud amounts, vertical structures, and optical properties. Section 4 compares the retrieved properties with the current MODIS product and the concluding remarks are given in section 5.

## 2. Data and methodology

### a. MODIS data

The MODIS imager is the principal instrument deployed on two National Aeronautics and Space Administration (NASA) Earth Observing System (EOS) satellites: *Terra* and *Aqua*. The imager has 36 onboard calibrated channels/bands (0.415–14.24  $\mu\text{m}$ ) (Barnes et al. 1998) at spatial resolutions of 250 m at nadir for two visible channels (bands 1 and 2), 500 m for five near-infrared channels (bands 3–7), and 1 km for bands 8–36. Global observations commenced in February 2000 for *Terra* and in June 2002 for *Aqua*. The data used in this study are 1-km aggregated radiance data (MOD021KM) from one visible (0.65 or 0.86  $\mu\text{m}$ ) and one infrared (11  $\mu\text{m}$ ) channel. Key additional variables employed are the MODIS-retrieved CO<sub>2</sub>-slicing-based altitude ( $P_c$ ) and ambient temperature of the cirrus cloud ( $T_c$ ) (Menzel et al. 2002; Platnick et al. 2003).

For cloud detection, this study relies on the MODIS level-2 cloud mask product generated by the MODIS cloud/clear-sky discrimination algorithm (Ackerman et al. 1998). The MODIS cloud-discriminating algorithm is in essence a series of cloud spectral tests applied to as many as 20 of the 36 MODIS channels, depending on surface scene types and solar illumination conditions. Four categories of cloud probability, namely, *confidence clear*, *probably clear*, *probably cloudy*, and *cloudy*, are identified at two spatial resolutions: 1-km and 5-km ( $5 \times 5$  pixels) scales. In this study, only 5-km

overcast scenes where all of the  $5 \times 5$  1-km pixels are identified as probably cloudy or cloudy are retrieved.

The MODIS  $P_c$  and  $T_c$  products are currently retrieved on a 5-km basis using two different approaches (Menzel et al. 2002; Platnick et al. 2003). If the CO<sub>2</sub>-slicing method retrieves a  $P_c$  less than 700 hPa, the CO<sub>2</sub>-slicing-retrieved  $P_c$  is used; otherwise, the cloud-top altitudes are inferred from the 11- $\mu\text{m}$  brightness temperature. The CO<sub>2</sub>-slicing method utilizes four MODIS infrared bands found in the CO<sub>2</sub> partial absorption regions, that is, band 33 (13.34  $\mu\text{m}$ ), band 34 (13.64  $\mu\text{m}$ ), band 35 (13.94  $\mu\text{m}$ ), and band 36 (14.24  $\mu\text{m}$ ). The method is considered to be effective in detecting thin cirrus clouds. It has been previously applied to the Visible Infrared Spin Scan-Radiometer (VISSR) Atmospheric Sounder (VAS) data (Wylie and Menzel 1989; Menzel et al. 1992) and HIRS data (Wylie et al. 1994; Wylie and Menzel 1999) and has demonstrated accuracies generally within  $\pm 50$  hPa for the retrieved high-cloud  $P_c$ .

For clouds with  $P_c \geq 700$  hPa, the CO<sub>2</sub>-slicing method loses its sensitivity and effectiveness so MODIS relies on the 11- $\mu\text{m}$  observed radiance to infer the low-cloud  $T_c$ . In this case, water vapor absorption/emission at 11  $\mu\text{m}$  can affect the low-cloud  $T_c$ , but the effect is generally small because the relative humidity above the cloud layer is usually small. Under moist conditions, the 11- $\mu\text{m}$  retrieved  $T_c$  can have biased errors of a few degrees. Once the  $T_c$  is retrieved, the  $P_c$  corresponding to the low cloud is inverted by comparing the profiles of  $P_c$  and  $T_c$  obtained from the National Centers for Environmental Prediction (NCEP) Global Data Assimilation System (Derber et al. 1991). A similar  $P_c$ -to- $T_c$  inversion is also applied to the  $P_c$  ( $<700$  hPa) determined by the CO<sub>2</sub>-slicing method.

### b. Overlapped retrieval algorithm

As mentioned earlier, the current MODIS product only provides the location of the tops of the highest cloud viewable from space, which poses a problem for overlapping clouds. To overcome this limitation, we apply the algorithm of Chang and Li (2005) to determine the existence of overlapped cirrus and water clouds and to retrieve their individual optical properties. The method is based on combined information from the multispectral CO<sub>2</sub>-slicing channels (13.3, 13.6, 13.9, and 14.2  $\mu\text{m}$ ) and conventional VIS and IR window channels. By taking full advantage of the MODIS products, our algorithm utilizes four essential pieces of information: 1) a high-cloud  $P_c/T_c$  ( $<500$  hPa) estimated from the CO<sub>2</sub>-slicing retrieval; 2) a low-cloud  $P_c/T_c$  ( $>500$  hPa) estimated from the mean of nearby low-cloud  $P_c/T_c$ ; 3) a high-cloud optical depth ( $\tau'_{VIS}$ ) estimated

based on 11- $\mu\text{m}$  emissivity; and 4) a total-column cloud optical depth ( $\tau_{\text{VIS}}$ ) estimated based on VIS reflectance (0.65  $\mu\text{m}$  for land and 0.86  $\mu\text{m}$  for oceans).

The algorithm was applied to only high-altitude ( $\text{Pc} < 500 \text{ hPa}$ ) thin cirrus clouds ( $\varepsilon_{\text{IR}} < 0.85$ , equivalent to  $\tau_{\text{VIS}} < 4$ ) to detect overlapping conditions. These conditions define the cirrus clouds in this study that represent the majority of cirrostratus and cirrocumulus clouds (Comstock and Sassen 2001; Sassen et al. 2003). The algorithm begins with a comparison between  $\tau_{\text{VIS}}$  and  $\tau'_{\text{VIS}}$ . To estimate  $\tau'_{\text{VIS}}$ , a parameterization scheme is followed by first computing an effective IR emissivity ( $\varepsilon_{\text{IR}}$ ) (Menzel et al. 1992; Wylie et al. 1994):

$$\varepsilon_{\text{IR}} = \frac{R - R_{\text{clr}}}{R_{\text{hc}} - R_{\text{clr}}}, \quad (1)$$

where  $R$  is the 11- $\mu\text{m}$  observed radiance,  $R_{\text{hc}}$  is the computed equivalent blackbody radiance at high-cloud Tc (from the CO<sub>2</sub>-slicing retrieval) and  $R_{\text{clr}}$  is the clear-sky radiance at the 11- $\mu\text{m}$  channel. An IR optical depth ( $\tau_{\text{IR}}$ ) is derived from  $\varepsilon_{\text{IR}}$  (Platt and Stephens 1980; Minnis et al. 1990):

$$\tau_{\text{IR}} = -\mu \ln(1 - \varepsilon_{\text{IR}}), \quad (2)$$

where  $\mu$  is the cosine of the satellite zenith angle. The high-cloud VIS optical depth ( $\tau'_{\text{VIS}}$ ) is obtained using the ratio factor  $\xi$  (Minnis et al. 1990; Rossow and Schiffer 1999), which relates the cirrus optical depths at the VIS and IR channels:

$$\tau'_{\text{VIS}} = \xi \tau_{\text{IR}}. \quad (3)$$

An observed mean value for  $\xi$ , equal to 2.13, is adopted for ice clouds following Minnis et al. (1993a) and Rossow and Schiffer (1999); it is also equal to a theoretical value for cloud models with hexagonal ice crystals (Takano and Liou 1989) and random fractal polycrystals (Mishchenko et al. 1996).

Because the parameterized  $\tau'_{\text{VIS}}$  is dictated by IR radiative transfer for the cirrus cloud and the VIS-retrieved  $\tau_{\text{VIS}}$  is dictated by the entire cloud column, the IR-based  $\tau'_{\text{VIS}}$  is significantly smaller than  $\tau_{\text{VIS}}$  if the cirrus cloud overlaps a low cloud. Figure 1a shows a typical case of  $\tau_{\text{VIS}}$  against  $\tau'_{\text{VIS}}$  retrievals for a cirrus cloud layer overlapping stratus clouds observed on 2 April 2001 over a 50-km region in north-central Oklahoma centered at the Southern Great Plains (SGP) Central Facility site (36.6°N, 97.5°W) of the U.S. Department of Energy Atmospheric Radiation Measurement (ARM) Program. The overlapping structure was confirmed by the ARM SGP ground-based measurements obtained from the Active Remotely Sensed Clouds Locations (ARSCL) product (Clothiaux et al. 2000). The differences between  $\tau'_{\text{VIS}}$  and  $\tau_{\text{VIS}}$  seen in

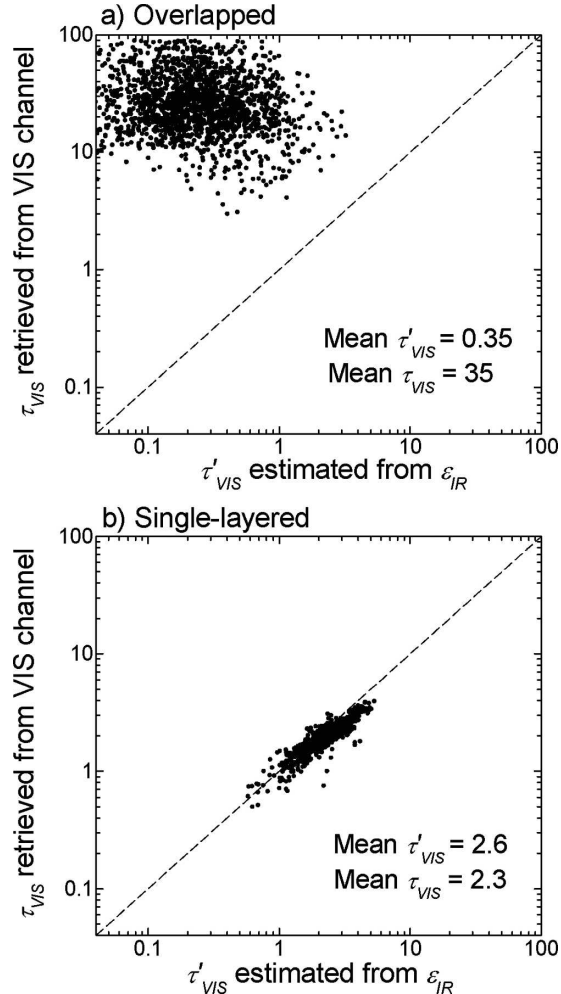


FIG. 1. Comparisons of  $\tau_{\text{VIS}}$  and  $\tau'_{\text{VIS}}$  for (a) overlapped cirrus and stratus clouds observed on 2 Apr 2001 (1715 UTC) and (b) single-layer cirrus clouds observed on 6 Mar 2001 (1735 UTC). The data are extracted from a 50-km MODIS region centered at the ARM SGP Central Facility site.

Fig. 1a are used to decide if a dual-layer overlapped cloud model should be called upon to retrieve separate optical properties for the cirrus and low-cloud layers. Figure 1b shows a typical case of a single-layer cirrus cloud (6 March 2001), that is,  $\tau'_{\text{VIS}} \approx \tau_{\text{VIS}}$ .

For an overlapped cloud case, the initial estimate of  $\varepsilon_{\text{IR}}$  from Eq. (1) needs to be corrected for the emission from the lower cloud (lc subscripts). This is achieved by replacing  $R_{\text{clr}}$  with an adjusted radiance term,  $R'$ :

$$R' = \varepsilon_{\text{lc}} R_{\text{lc}} + (1 - \varepsilon_{\text{lc}}) R_{\text{clr}}, \quad (4)$$

where  $R_{\text{lc}}$  is the computed low-cloud blackbody emission radiance at low-cloud Tc, and  $\varepsilon_{\text{lc}}$  is the low-cloud 11- $\mu\text{m}$  emissivity. The optical properties of the low clouds were determined by assuming that the low clouds

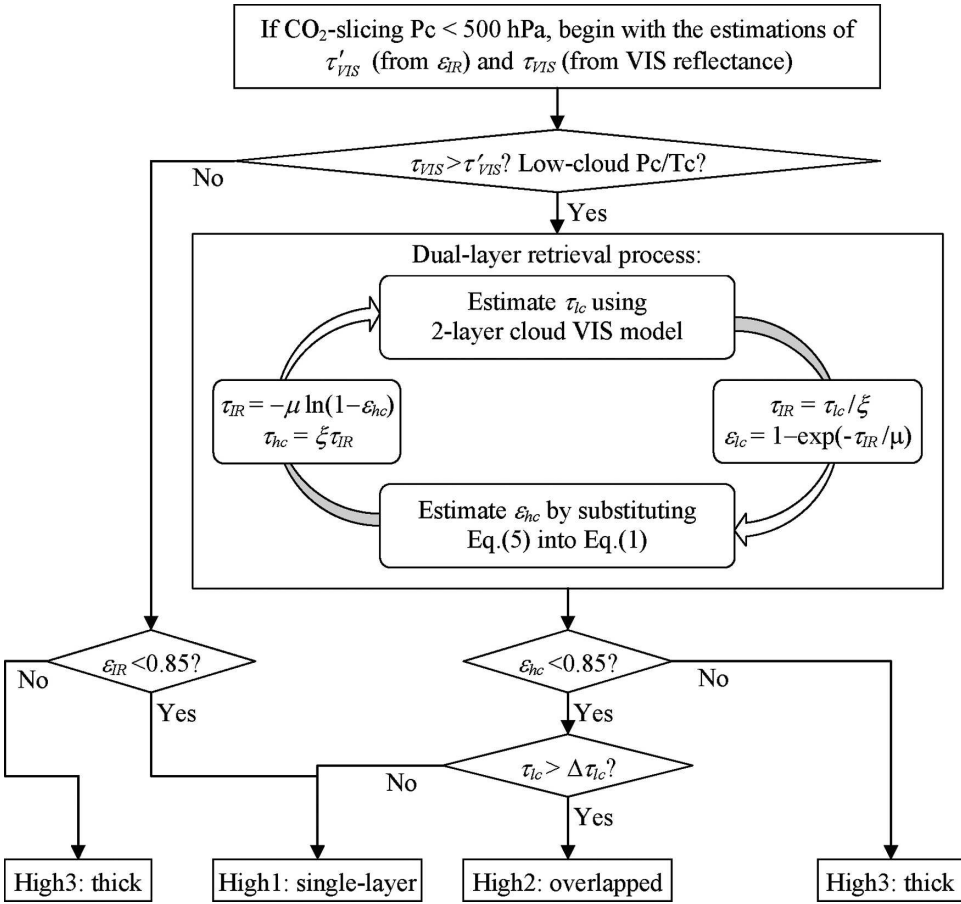


FIG. 2. A schematic flowchart illustrating the retrieval algorithm.

detected nearby were from the same low-cloud system. Within a maximum area of ±125 km for a typical mesoscale cloud system, neighboring low-cloud pixels (with P<sub>c</sub> > 500 hPa) were examined. If no single-layer low cloud existed within this domain, no retrieval was made for the overlapped cloud, even though τ<sub>VIS</sub> may have been larger than τ'<sub>VIS</sub>. Such cases that accounted for ∼5% of the 4-month's worth of data were assumed single-layer clouds.

When all three conditions are met, that is, P<sub>c</sub> < 500 hPa, τ<sub>VIS</sub> > τ'<sub>VIS</sub>, and there exists neighboring low cloud, a dual-layer cirrus-over-water cloud radiative transfer model is applied to the VIS channel to retrieve a low-cloud optical depth (τ<sub>lc</sub>). Initially, the ε<sub>IR</sub>-based τ'<sub>VIS</sub> is used in the dual-layer cloud model. The best-fit value of τ<sub>lc</sub> is determined by adjusting τ<sub>lc</sub> until the model-computed VIS reflectance matches with the observation. From Eq. (3), τ<sub>lc</sub> is converted to a low-cloud τ<sub>IR</sub> by using an empirical value of ξ = 2.56 for water clouds (Minnis et al. 1993a; Rossow and Schiffer 1999). The low-cloud emissivity ε<sub>lc</sub> is estimated from Eq. (2).

By substituting Eq. (4) into Eq. (1) for R<sub>clr</sub>, our nominal high cloud ε<sub>hc</sub> is expressed as

$$\epsilon_{hc} = \frac{R - R'}{R_{hc} - R'}. \quad (5)$$

Likewise, our nominal high-cloud optical depth (τ<sub>hc</sub>) can be obtained from ε<sub>hc</sub> using Eqs. (2) and (3). Because the retrievals of τ<sub>hc</sub> and τ<sub>lc</sub> are mutually dependent, an iterative process is needed.

From the retrieved ε<sub>hc</sub> and P<sub>c</sub>, all high clouds with P<sub>c</sub> < 500 hPa are classified into three categories: 1) High1: single-layer cirrus clouds, 2) High2: cirrus overlapping low clouds, and 3) High3: thick high clouds (ε<sub>hc</sub> ≥ 0.85). Figure 2 shows a flowchart illustrating our processing paths for High1, High2, and High3 clouds. The High3 category includes two processing paths with (rightmost path) and without (leftmost path) the identification of nearby low cloud. In either case, the High3 cloud is considered as a single thick layer cloud with a total-column τ<sub>VIS</sub>. But in nature, some High3 clouds are probably overlapped.

TABLE 1. Cloud categories.

High1	Single-layer cirrus cloud
High2	Overlapped cirrus cloud
High3	Thick high cloud
Mid	Middle cloud
Low1	Single-layer low cloud
Low2	Overlapped low cloud

For all lower clouds with  $P_c \geq 500$  hPa, no decision was made regarding overlapping. They are separated into a Low1 category for  $P_c > 600$  hPa and an ad hoc Mid category for  $500 \text{ hPa} \leq P_c \leq 600$  hPa. Selection of this interval for the Mid category was mainly to illustrate an extremely low occurrence of MODIS  $P_c$  falling between 500 and 600 hPa as revealed in this study. The zonal-mean percentage of the occurrence of Mid clouds, which may be overlapped with cirrus or low clouds, is equal to 1%–2% in low and midlatitudes. Table 1 lists six cloud categories, namely, High1, High2, High3, Mid, Low1, and Low2. The retrieved lower clouds overlapped by High2 are hereafter referred to as Low2.

### c. Lookup tables and dual-layer radiative transfer calculations

Our algorithm is implemented by means of lookup tables in order to accelerate the processing of large volumes of data. Lookup tables of radiances are obtained from extensive radiative transfer simulations for a two-layer cloud model with overlapped ice and water clouds. Using various inputs of high-cloud and low-cloud optical properties, the tables were generated by running a 32-stream adding-doubling code (Chang and Li 2002). The input values are for high clouds  $\tau_{hc} = 0.01, 0.25, 0.5, 1, 2, 3$ , and 5, and  $P_c = 100, 300$ , and 500 hPa and for low clouds  $\tau_{lc} = 0.05, 0.25, 1, 2, 3, 4, 6, 8, 12, 16, 24, 32, 40, 48, 56, 64, 80$ , and 100, and  $P_c = 500, 700, 900$ , and 1000 hPa. The atmosphere is divided into 10 vertical layers and each layer is 100 hPa thick. Both high and low clouds are inserted at each  $P_c$  level as an infinitesimal plane-parallel layer.

Our microphysical model for high clouds assumes an ice cloud layer with a fixed effective radius of  $r_e = 30 \mu\text{m}$  and adopts the scattering phase functions of the fractal ice polycrystal model (Macke 1993; Mishchenko et al. 1996). This microphysical model for high clouds is the same as the ISCCP ice cloud model (Rossow and Schiffer 1999), as shown by a series of comparisons against observational data (Minnis et al. 1993b; Francis 1995; Descloitres et al. 1998). For example, Descloitres et al. (1998) show that the observed angular distributions of the visible reflectances from cirrus clouds agree

within a few percent with calculations based on the fractal-polycrystal scattering phase functions. The optical refractive indices used for ice clouds are  $1.332 + 1.672 \times 10^{-8}i$  for  $0.65 \mu\text{m}$  and  $1.329 + 3.290 \times 10^{-7}i$  for  $0.86 \mu\text{m}$  (Warren 1984). Our microphysical model for low clouds assumes a fixed droplet effective radius of  $r_e = 10 \mu\text{m}$  and adopts Mie scattering phase functions, again the same as the ISCCP water cloud model. The optical refractive indices used for water clouds are  $1.332 + 1.672 \times 10^{-8}i$  for  $0.65 \mu\text{m}$  and  $1.329 + 3.290 \times 10^{-7}i$  for  $0.86 \mu\text{m}$  (Hale and Querry 1973). The assumptions made concerning cloud microphysics may incur uncertainties in the retrieved optical depths on the order of 30%–50% for thin ice clouds (Rossow et al. 1989; Minnis et al. 1993b) and on the order of 15%–25% for thicker water clouds (Rossow et al. 1989).

Atmospheric transmittance and molecular scattering are calculated using the MODTRAN-4 model with the *U.S. Standard Atmosphere, 1976* (COESA 1976) temperature and humidity profiles (Berk et al. 1999). Surface albedos over land were obtained from the bi-monthly MODIS Filled Land Surface Albedo Product. For oceanic scenes, the surface albedo is 0.05. No retrievals were attempted for regions of snow-/ice-covered surfaces (e.g., polar regions), sun-glint water, and mountainous areas because of large uncertainties in the surface properties. The snow/ice surface data are reported by the National Snow and Ice Data Center's Near-real-time Ice and Snow Extent (Armstrong and Brodzik 2001) and are included in the MODIS 1-km Quality Assurance data (Platnick et al. 2003). Small uncertainties ( $\pm 10\%$ ) in surface albedo and atmospheric properties have little impact on the retrievals when the total-column  $\tau_{VIS}$  is moderately large ( $> 5$ ). Since the retrieval of high cloud  $\tau_{hc}$  relies primarily on the CO<sub>2</sub>-slicing and 11-μm IR channels, uncertainties in the surface albedo have little effect on its retrieval. The uncertainties have more influence on the retrieved low-cloud  $\tau_{lc}$  because this retrieval primarily relies on the VIS channel. For example, uncertainties of 3% in the VIS reflectance can lead to uncertainties of  $\sim 1.0$  in moderate  $\tau_{lc}$  retrievals. Uncertainties due to neglecting the water vapor effects above the cloud at the 11-μm IR channel can cause biases in the retrieved  $\tau_{hc}$  and  $\varepsilon_{hc}$ , but they are estimated to be no more than 10%.

## 3. Near-global cloud properties

### a. Cloud amounts and 5-km overcast scenes

The MODIS data used in this study are from measurements made by the *Terra* satellite (nominal overpass time 1030 local time) during January, April, July, and October 2001. Global data were processed exclud-

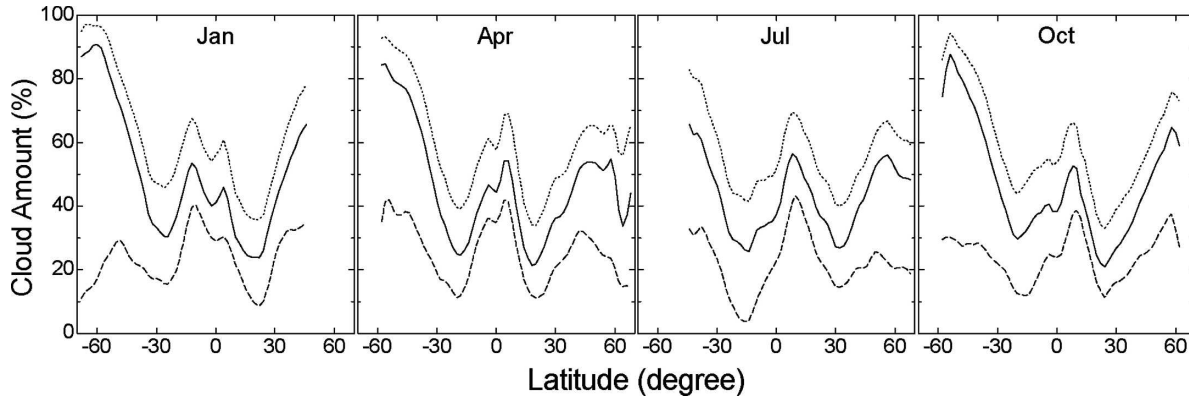


FIG. 3. Latitudinal variations of the zonal-mean total cloud amount (dotted), total 5-km overcast cloud amount (solid), and total 5-km overcast high-cloud ( $P_c < 500 \text{ hPa}$ ) amount (dashed) obtained in January, April, July, and October 2001.

ing polar winter regions and solar zenith angles greater than  $75^\circ$ . The data are sampled every fourth day in each month (i.e., day 2, 6, 10, 14, 18, 22, 26, and 30). Note that operation of the *Terra/MODIS* instrument was interrupted between mid-June and 2 July 2001, so data on 4 July was used instead of 2 July. Use of the sampled data is necessary to reduce the data volume, while providing reasonable global cloud characteristics since synoptic weather systems transit on a time scale of  $\sim 4\text{--}7$  days. There is a potential bias due to the diurnal variation of clouds.

Figure 3 shows the latitudinal variations of  $1^\circ$  zonal-mean total cloud amount (dotted), total 5-km overcast amount (solid), and total 5-km overcast high-cloud ( $P_c < 500 \text{ hPa}$ ) amount (dashed) obtained from MODIS in January, April, July, and October 2001. The near-global monthly mean total cloud amounts are around 60% with the lowest occurring in July (~57%) and the highest occurring in January (~61%). The corresponding overcast total cloud amounts are about 45% (~48% in

January and ~42% in July). The smaller cloud amounts in July are consistent with the results from ISCCP and HIRS (cf. Table 2 in Jin et al. 1996), except that the MODIS monthly mean total cloud amounts are generally smaller. The 5-km overcast cloud amount exhibits a similar latitudinal variation to that of the total cloud amount. The patterns of the latitudinal variations are also similar to those derived from ISCCP and HIRS (Rossow and Schiffer 1999; Jin et al. 1996).

Wylie et al. (1994) and Jin et al. (1996) reported that the annual-mean total cloud amounts from HIRS were equal to 76%–77%. Jin et al. (1996) and Rossow and Schiffer (1999) reported an annual-mean total cloud amount equal to 63% based on the previous version of the ISCCP C-series dataset; the annual-mean total cloud amount increases to 68% using the new ISCCP D-series dataset. Stowe et al. (2002) and Jacobowitz et al. (2003) compared monthly means from 10-yr (1985–94) cloud climatologies compiled from ISCCP data and the Clouds from AVHRR (CLAVR) dataset

TABLE 2. Absolute cloud amounts and relative percentage of High1, High2, High3, Mid, and Low1 clouds obtained for over ocean/land in January, April, July, and October 2001.

	Jan 2001	Apr 2001	Jul 2001	Oct 2001	Mean
Absolute (%)					
High1	4.3/5.5	4.6/4.8	3.4/3.7	4.0/5.2	4.1/4.8
High2	12.3/14.0	14.3/12.6	9.9/9.0	12.8/12.7	12.3/12.1
High3	7.6/9.3	7.9/7.6	7.2/7.6	7.9/9.1	7.6/8.4
Mid	2.3/1.4	1.2/1.0	1.8/2.2	1.5/1.1	1.7/1.4
Low1	22.4/13.6	18.8/14.0	20.4/16.2	20.6/14.5	20.6/14.6
Relative (%)					
High1	8.8/12.5	9.9/11.9	7.9/9.5	8.6/12.2	8.8/11.5
High2	25.2/32.0	30.5/31.5	23.3/23.4	27.2/29.8	26.6/29.2
High3	15.6/21.2	16.9/18.9	16.8/19.6	16.9/21.3	16.6/20.2
Mid	4.6/3.2	2.6/2.6	4.3/5.6	3.3/2.6	3.7/3.5
Low1	45.8/31.1	40.1/35.1	47.7/42.0	44.0/34.1	44.4/35.6

of the NOAA AVHRR Pathfinder Atmosphere Project (PATMOS) and found rather constant 48%–52% total cloud amounts. These differences are caused by different cloud detection techniques used by the different groups. For example, Stowe et al. (2002) suggest that CLAVR tends to be more conservative in preserving the overcast radiances so a large portion of variable cloudy pixels were classified as mixed pixels and were assigned 50% cloud coverage. ISCCP tends to treat them as completely overcast with 100% cloud coverage. Our results imply that the MODIS total cloud amount falls somewhere between the ISCCP and CLAVR total cloud amounts. The HIRS monthly mean high-cloud amounts reported by Wylie et al. (1994) and Jin et al. (1996) are equal to 35%. The MODIS high-cloud amount (all clouds with  $P_c < 500 \text{ hPa}$ ) is equal to 24% for 5-km overcast pixels and 32% for all pixels. The HIRS total cloud amounts may be overestimated due to its much larger pixel size ( $\sim 20 \text{ km}$  at nadir).

Figure 4 shows the variations of the  $1^\circ$  zonal-mean 5-km overcast amounts for each of the five categories (i.e., High1, High2, High3, Low1, and Mid) obtained over ocean/land in April 2001. The patterns for other months are similar except that they shift with the position of the sun. Table 2 shows the global monthly means of the five cloud categories in terms of absolute cloud amount (upper rows) and relative percentage (lower rows) out of the total 5-km overcast amounts for each of the 4 months. Considerably more clouds are found over oceans than over land. The two most dominant categories are Low1 (single-layer low clouds) and High2 (overlapped cirrus clouds). The overlapped High2 clouds account for about 50% of total high clouds and 30% of total overcast amounts. This result is consistent with ship observations, which note that cirrus clouds rarely occur alone over oceans (Warren et al. 1985). The true overlapped high-cloud amounts should be even larger because a fraction of High3 may be overlapped but cannot be identified. In general, high clouds occur most frequently over the ITCZ and midlatitudes and less frequently in the subtropics. Tropical high clouds are often associated with extensive anvil cirrus clouds covering large spatial domains. At higher latitudes, they are accompanied by storms and fronts, as revealed from ground observations (e.g., Warren et al. 1985). There are more High3 clouds in low latitudes due to tropical convection and in midlatitudes due to mesoscale cyclones. Relatively more frequent high clouds are found over land than over ocean, but the total high-cloud amounts are similar ( $\sim 25\%$ ).

Table 2 also reveals that there are fewer low clouds (Low1) than total high clouds (High1 + High2 + High3), especially over land. This is because with sat-

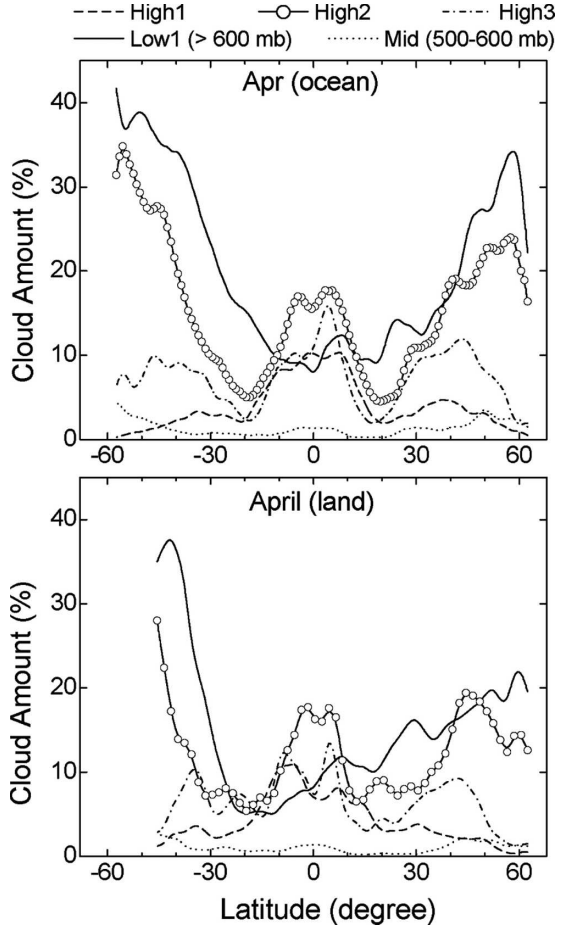


FIG. 4. Latitudinal variations of zonal-mean overcast cloud amounts for High1, High2, High3, Mid, and Low1 over (top) ocean and (bottom) land obtained in April 2001.

ellite views from above the atmosphere, the presence of high clouds can obscure lower clouds. In regions of prevailing high clouds, all potential lower clouds would be missed by a single-layer assumption, leading to underestimated low-cloud amounts. Our overlapped retrievals of the High2 clouds “recover” a large fraction of the overlapped Low2 clouds.

#### b. A bimodal distribution of cloud $P_c$ vertical structure

Figure 5 shows the monthly frequency distributions of  $P_c$ , normalized to 100%, for all overcast clouds (solid lines) obtained in April 2001. A distinct bimodal distribution of  $P_c$  is seen with a demarcation at about 500 hPa. Almost identical bimodal  $P_c$  distributions are found in the other 3 months (January, July, and October). To better display the cloud vertical structure, Fig. 5 plots the  $P_c$  distributions for 1) single-layer Low1, Mid, and High1 clouds (connected with the same

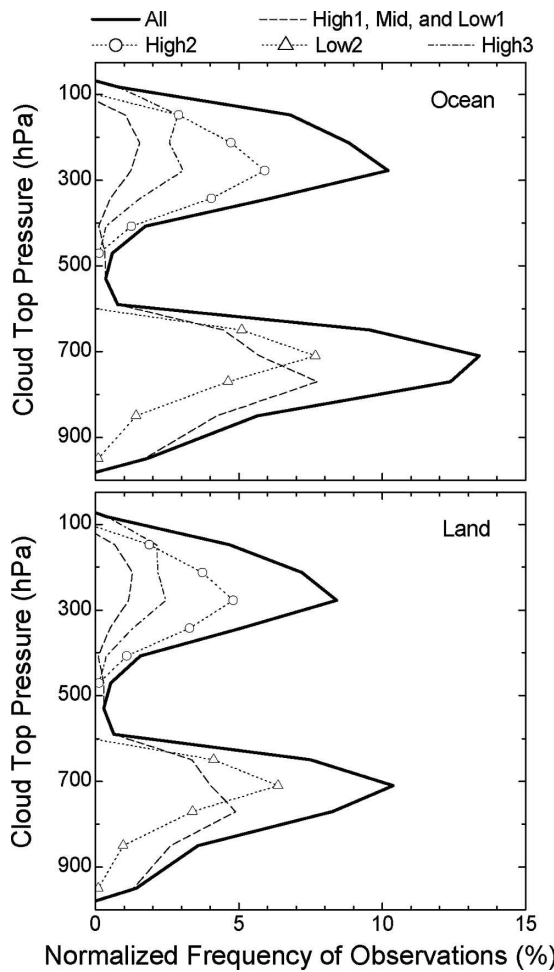


FIG. 5. Normalized frequencies of  $P_c$  observations for all 5-km overcast clouds (100%) (thick solid lines) and for High1, Mid, Low1 (connected with dashed lines), High2 (dashed lines with circles), Low2 (dashed lines with triangles), and High3 (dash-dotted) obtained over (top) ocean and (bottom) land in April 2001.

dashed curves); 2) overlapped High2 (dotted lines with circles) and Low2 (dotted lines with triangles) clouds; and 3) thick High3 (dash-dotted lines). Note that Low2 and High2 are from the same overlapped cloud configuration; they have the same total frequency but different  $P_c$ . It should be pointed out that the bimodal  $P_c$  distribution does not result from our dual-layer cloud retrievals. As seen from Fig. 5, the MODIS standard cloud-top product reveals the same bimodal distribution without the inclusion of our Low2 clouds. It is this bimodal  $P_c$  distribution that forms the foundation of our overlapped cloud retrieval algorithm.

The bimodal  $P_c$  distribution shows two maxima at around 275 and 725 hPa corresponding to two typical cloud types: 1) low-level boundary clouds, like stratus, shallow cumulus, and stratocumulus (Kuettner 1971;

Agee 1984), and 2) high-level clouds resulting from synoptic weather systems, like midlatitude fronts and cyclones and tropical storms and anvils (Starr and Cox 1985; Sheu et al. 1997). Also, there is a universal minimum between 500 and 600 hPa. When including all MODIS  $P_c$  data, that is, not limited to the 5-km overcast pixels, we found less than 4% of clouds having  $P_c$  between 500 and 600 hPa. Since our algorithm cannot retrieve more than two layers of clouds, the retrieved low clouds may represent the average of all layers of clouds beneath the cirrus. Resolving multilayer low clouds is not possible at the moment unless ground-based or spaceborne radar are used (Mace et al. 2001; Stephens et al. 2002).

The occurrence of a minimum in  $P_c$  is similar to the finding of minimum cloudiness from previous sounding data obtained during the Tropical Ocean Global Atmosphere Coupled Ocean–Atmosphere Response Experiment (TOGA COARE; Zuidema 1998). Comstock and Jakob (2004) also revealed such dominant high- and low-cloud regimes when comparing the ARM ground-based ARSCL measurements with those predicted by the European Centre for Medium-Range Weather Forecasts (ECMWF) model in the tropical western Pacific between April and November of 1999. In other studies concerning the distribution of tropical convective clouds, high-top clouds ( $>5$  km) are divided into two categories: cumulus congestus ( $<10$  km) and deep cumulonimbus ( $>10$  km). This suggests the trimodal nature of tropical cumulus cloud types if shallow cumulus (cloud tops near 2 km) are included (Liu and Moncrieff 1998; Johnson et al. 1999). Unfortunately, MODIS cannot differentiate between more than two layers of clouds. On the other hand, the fact that the MODIS  $P_c$  product representing the top of the highest clouds seen from space has a clear bimodal distribution is a testimony to the fact that the bimodal  $P_c$  distribution is predominant on a global scale. Understanding this ubiquitous vertical structure is important because cloud vertical distribution influences the radiative and latent heating profiles of the atmosphere, which in turn influences both small-scale and large-scale dynamics and the atmospheric general circulation (Ramaswamy and Ramanathan 1989; Randall et al. 1989; Sherwood et al. 1994). More verification of the global cloud vertical structure is thus required.

Figure 6 shows the monthly frequency distribution of cloud optical depth ( $\tau_{\text{VIS}}$ ) for the single-layered and overlapped cloud categories and their total. The bin selections of the optical depth intervals follow the ISCCP (Rossow and Schiffer 1999), that is, 0–1.3, 1.3–2.2, 2.2–3.6, 3.6–5.8, 5.8–9.4, 9.4–14.8, 14.8–23, 23–36, and 36–60. The mean  $P_c$ ,  $T_c$ , and  $\tau_{\text{VIS}}$  calculated for all

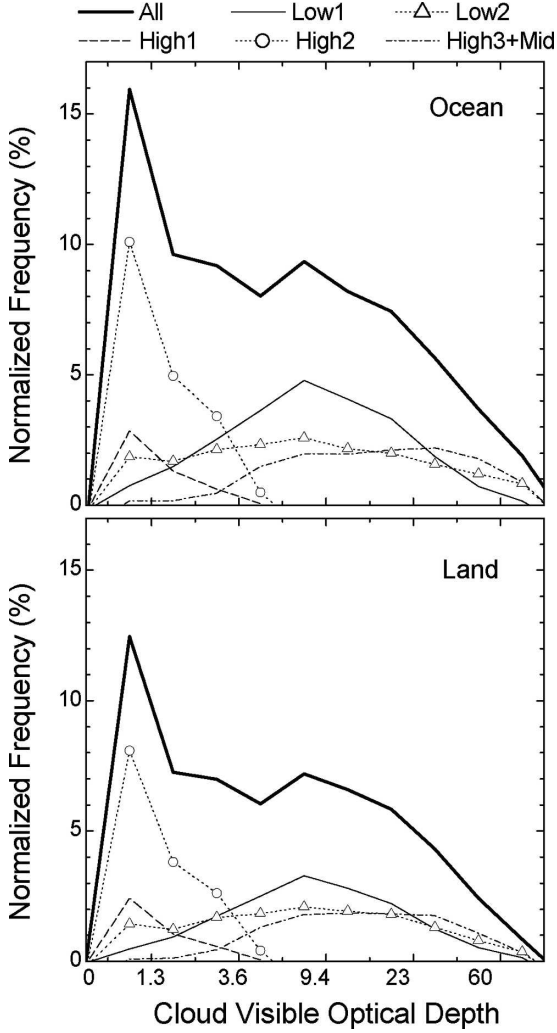


FIG. 6. As in Fig. 5 but for normalized frequencies of  $\tau_{\text{VIS}}$  observations for all 5-km overcast clouds (100%) (thick solid lines) and for Low1 (thin solid lines), Low2 (dashed lines with triangles), High1 (dashed), High2 (dashed lines with circles), and High3 + Mid (dash-dotted).

months are given in Table 3. Clearly, cirrus clouds from single-layer (High1) and overlapped (High2) categories have the smallest  $\tau_{\text{VIS}}$  among all cloud types, with means equal to  $\sim 1.5$  and standard deviations equal to  $\sim 1.0$ . A large number of high-cloud  $\tau_{\text{VIS}}$  peak at  $\sim 1.0$ , which is dominated by cirrus clouds that overlap with low clouds. This result agrees with the earlier reports by ship observers that cirrus clouds rarely occur alone over the oceans (Warren et al. 1985). The distributions of Low1 and Low2  $\tau_{\text{VIS}}$  are much broader with similar means ( $\pm$  standard deviations) of  $\sim 11$  ( $\pm 10$ ) for Low1 clouds and  $\sim 14$  ( $\pm 13$ ) for Low2 clouds. It is also found that High3 clouds have the largest mean  $\tau_{\text{VIS}} \sim 22$  (standard deviations  $\sim 20$ ) and Mid clouds ( $P_c = 500$ –600

TABLE 3. Monthly mean  $P_c$ ,  $T_c$ , and  $\tau_{\text{VIS}}$  for High1, High2, High3, Mid, Low1, and Low2 and monthly mean  $\varepsilon_{hc}$  for High1, High2, and High3 obtained for ocean/land in each month. The last column is the 4-month overall mean.

	Jan 2001	Apr 2001	Jul 2001	Oct 2001	Mean
$P_c$ (hPa)					
High1	285/253	262/263	289/293	283/262	280/268
High2	322/292	307/300	322/324	320/302	318/304
High3	285/252	265/261	276/280	271/254	274/262
Mid	556/558	555/558	556/557	555/558	556/558
Low1	757/759	762/754	762/756	758/763	760/758
Low2	705/705	712/706	706/700	707/708	708/705
$T_c$ (K)					
High1	229/225	226/226	233/234	230/228	230/228
High2	236/232	234/233	238/240	236/235	236/235
High3	229/224	226/225	230/231	227/226	228/227
Mid	264/267	264/265	267/268	264/266	265/267
Low1	278/280	278/278	280/281	278/280	279/280
Low2	276/277	276/276	278/278	276/278	277/277
$\tau_{\text{VIS}}$					
High1	1.45/1.38	1.35/1.39	1.51/1.57	1.40/1.41	1.43/1.44
High2	1.60/1.47	1.40/1.40	1.63/1.67	1.55/1.54	1.54/1.52
High3	21.1/21.2	22.4/19.0	23.1/22.3	22.6/21.4	22.3/21.0
Mid	15.9/13.8	16.5/14.8	17.5/17.0	17.9/15.2	17.0/15.2
Low1	10.8/10.1	10.7/10.6	10.4/10.8	11.1/10.6	10.8/10.5
Low2	13.3/12.2	14.3/12.6	13.8/13.9	14.0/13.4	13.8/13.0
$\varepsilon_{hc}$					
High1	0.52/0.51	0.50/0.51	0.54/0.55	0.51/0.52	0.52/0.52
High2	0.54/0.51	0.49/0.49	0.55/0.56	0.53/0.53	0.53/0.52
High3	0.92/0.91	0.91/0.91	0.92/0.92	0.92/0.92	0.92/0.92

hPa) have the second largest mean  $\tau_{\text{VIS}} \sim 16$  (standard deviations  $\sim 20$ ).

Figure 7 compares the joint frequency distributions of  $P_c$  and  $\tau_{\text{VIS}}$  derived from the standard MODIS products (Fig. 7a) and our retrievals (Fig. 7b) for the 4-month total overcast amounts (46% over ocean and 41% over land). The MODIS products shown in Fig. 7a represent the single-layer cloud retrievals whereas Fig. 7b includes both our single-layer and overlapped retrievals obtained from the same data as shown in Fig. 7a. Both  $P_c$  and  $\tau_{\text{VIS}}$  intervals follow the ISCCP bin intervals (Rossow and Schiffer 1991). The overcast amounts for  $P_c < 500$  hPa and  $P_c \geq 500$  hPa are given separately over ocean (left panels) and over land (right panels). It should be emphasized that the MODIS cloud-top products only provide the height of the top-most cloud layer as viewed from space. Through our retrieval, approximately half of the high-top clouds (12% out of 24% over ocean and 12% out of 25% over land) contain overlapped low clouds. Over ocean, the total low-cloud amount has increased from 22% for the MODIS retrieval (Fig. 7a) to 34% for our retrieval (Fig. 7b); over land, the increase is from 16% for the MODIS retrieval (Fig. 7a) to 28% for our retrieval (Fig. 7b). If

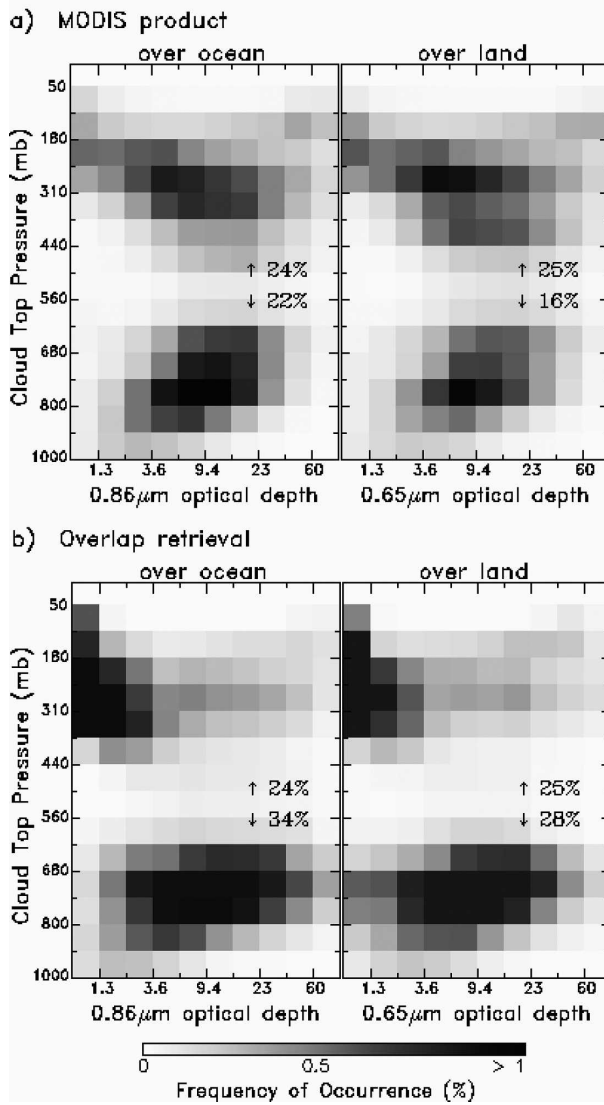


FIG. 7. Joint frequency distributions of  $P_c$  and  $\tau_{VIS}$  for the 4-month total overcast clouds from (a) the MODIS standard products and (b) current overlapped retrievals. Results are obtained separately for (left) over ocean and (right) over land. The numbers in each subpanel indicate the overcast cloud amounts with  $P_c < 500$  hPa ( $\uparrow$ ) and  $P_c \geq 500$  hPa ( $\downarrow$ ).

one uses the MODIS cloud-top data alone to determine the high-cloud and low-cloud amounts, the low-cloud fractions would be substantially underestimated.

Since the MODIS  $\tau_{VIS}$  is retrieved for the entire cloud column, attributing  $\tau_{VIS}$  to a single cloud top at  $P_c$  would substantially overestimate the cirrus optical depth when overlapping a low cloud. Another bias may also arise in choosing a single cloud microphysical model for the overlapped ice over water clouds. Assuming such overlapped clouds as single-layer ice or water clouds can lead to significant biases.

### c. Latitudinal distributions of $P_c$ , $T_c$ , and $\tau_{VIS}$

Figure 8 shows the variations of zonal-mean  $P_c$ ,  $T_c$ , and  $\tau_{VIS}$  corresponding to each of the six cloud categories in April of 2001. The main features of these zonal-mean  $P_c$ ,  $T_c$ , and  $\tau_{VIS}$  shift with seasons but are similar. From Fig. 8a, mean  $P_c$  for the High1, High2, and High3 clouds vary between 200 and 350 hPa; it is highest ( $\sim 200$  hPa) in the Tropics due to deep convection and lower toward higher latitudes due to a lower tropopause. Mean  $P_c$  for Low1 and Low2 clouds vary mostly between 700 and 800 hPa with less latitudinal variability. The mean  $P_c$  for the Mid cloud is nearly constant at  $\sim 550$  hPa, mainly because of the narrow  $P_c$  interval defined for this cloud type. From Fig. 8b, the high clouds are found mostly between 215 and 240 K with the lowest  $T_c$  in the Tropics ( $\sim 215$  K). The values of  $P_c$

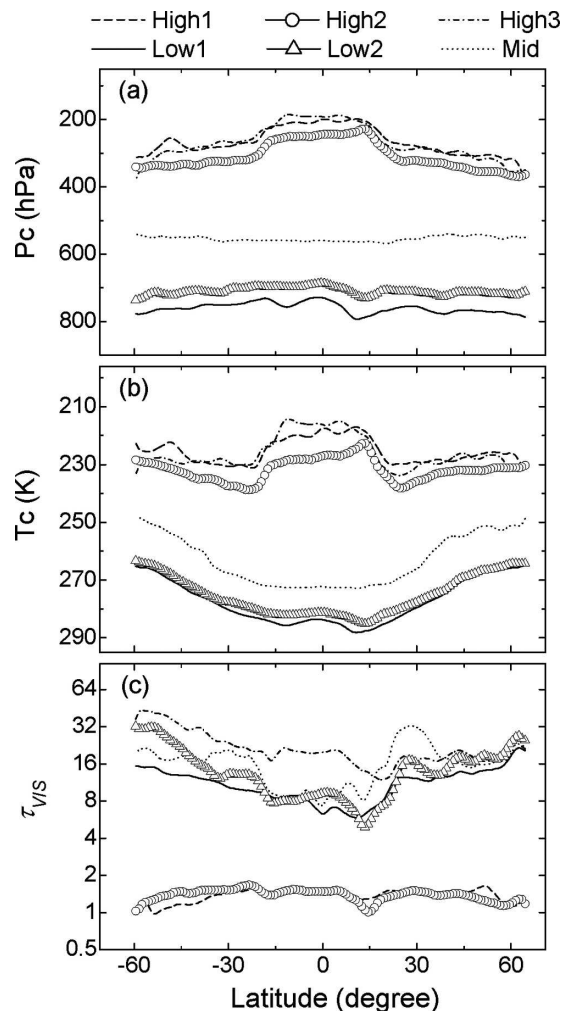


FIG. 8. Latitudinal variations of zonal-mean (a)  $P_c$ , (b)  $T_c$ , and (c)  $\tau_{VIS}$  for High1, High2, High3, Mid, Low1, and Low2 in April 2001.

and Tc for high clouds perceptibly change around 20°–30° in both hemispheres and this is attributed to the subtropical subsidence regions. The decreases of high-cloud Tc beyond 30° are affected by both the decreases of the earth's surface temperature and atmospheric temperature toward the polar regions. This is also the case for low clouds (Mid as well), where mean low-cloud Tc decreases progressively from ~285 K in the Tropics to less than 270 K at 60°N and 60°S. Differences between high-cloud and low-cloud Pc/Tc are largest in the Tropics and smaller toward higher latitudes. The standard deviations for these high- and low-cloud categories are similar with ~100 hPa for their mean Pc and ~7 K for their mean Tc.

It is worth noting that the mean Pc and Tc of High2 clouds are systematically larger (lower in altitude) than those of High1 and High3, and the Pc and Tc of Low2 are smaller (higher in altitude) than those of Low1. The differences are about  $\Delta$ Pc  $\sim$  40–50 hPa and  $\Delta$ Tc  $\sim$  3–7 K on a near-global average as shown in Table 3. We suspect that the differences for high clouds stem from the single-layer cloud assumption adopted in the MODIS CO<sub>2</sub>-slicing retrievals that do not take into account the influence of the underlying low clouds. Baum and Wielicki (1994) found that such errors depend on the lapse rate between the low-cloud and surface temperatures. Our results also revealed a larger  $\Delta$ Pc in the Tropics (where surface temperatures are more than 15 K larger than the low-cloud Tc), but generally smaller  $\Delta$ Pc at higher latitudes (where surface temperatures are closer to the low-cloud Tc,  $\Delta$ T  $<$  7 K). The differences between Low2 and Low1 Tc are likely due to the following two reasons: 1) contamination from undetected cirrus clouds resulting in smaller Tc and Pc, and 2) as all Low2 clouds are accompanied by the High2 clouds, the Low2 may have developed higher with a larger vertical extent (smaller Pc/Tc) than the more uniform single-layer Low1 clouds. Unfortunately, we cannot verify if either or both are the causes.

In comparisons of the zonal-mean  $\tau_{\text{VIS}}$  (Fig. 8c), High1 and High2 clouds have the smallest  $\tau_{\text{VIS}}$  (~1.0–1.8), which is expected for cirrus clouds with  $\varepsilon_{\text{hc}} < 0.85$ . Table 3 shows that there is little difference in terms of monthly means between High1 (~1.3–1.5) and High2 (~1.4–1.7) clouds. Some dips in the High2  $\tau_{\text{VIS}}$  (e.g., near 15°) are associated with small cloud amounts due to sparse data sampling. Among all cloud categories, thick High3 clouds have the largest  $\tau_{\text{VIS}}$  on average ( $\sim 22 \pm 20$ ); Mid clouds have the second largest  $\tau_{\text{VIS}}$  ( $\sim 16 \pm 20$ ); and Low1 ( $\sim 11 \pm 10$ ) and Low2 ( $\sim 14 \pm 13$ ) clouds have relatively smaller  $\tau_{\text{VIS}}$ . These differences are mainly due to the different geometrical vertical extents of high, mid-, and low clouds. The Mid  $\tau_{\text{VIS}}$

exhibits the largest latitudinal variability due to its fewest cloud amounts. The Low2  $\tau_{\text{VIS}}$  is generally larger than the Low1  $\tau_{\text{VIS}}$ , which is probably because the Low2 clouds near high clouds are geometrically thicker than those more uniform Low1 clouds or probably because those Low2 clouds contained cirrus as mentioned earlier. The latitudinal variations of Low1 and Low2  $\tau_{\text{VIS}}$  somewhat follow their zonal-mean cloud amounts as shown in Fig. 4.

Low-cloud  $\tau_{\text{VIS}}$  are on average smaller at low latitudes than at higher latitudes because there are more small stratocumulus clouds in the Tropics and more large stratus cloud systems in the midlatitudes. The ISCCP data also show similar finding (Tselioudis et al. 1992; Rossow and Schiffer 1999). Satellite and ship measurements show that overall  $\tau_{\text{VIS}}$  is larger for stratus clouds and smaller for cumulus clouds (Pincus et al. 1999). The presence of ice clouds that were assumed to be liquid water clouds may also explain the increase in  $\tau_{\text{VIS}}$  toward higher latitudes (Rossow and Schiffer 1999). The High3 clouds generally have the largest  $\tau_{\text{VIS}}$  among all cloud categories. They also tend to be larger toward higher latitudes. Previous analyses of high spatial-resolution Landsat data show that the satellite-retrieved  $\tau_{\text{VIS}}$  in convective cloud fields are, in fact, dominated by clouds with small optical depths (Wielicki and Parker 1992). The horizontal variability of  $\tau_{\text{VIS}}$  is greater for tropical clouds than for midlatitude clouds. Also, the midlatitude High3 clouds are often nimbostratus and dense cirrostratus clouds associated with mesoscale cyclones (e.g., the South Pacific convergence zone). This may explain the larger High3  $\tau_{\text{VIS}}$  found in southern midlatitudes. These differences may also be due to the assumption of a plane-parallel cloud. However, these latitudinal variations would require further verification.

#### *d. Geographical distributions of overcast cloud amount*

The near-global distributions of monthly mean overcast cloud amount obtained within  $1^\circ \times 1^\circ$  grid boxes for January, April, July, and October of 2001 are shown in Fig. 9a for all high clouds (High1 + High2 + High3), in Fig. 9b for cirrus clouds (High1 + High2), and in Fig. 9c for overlapped cirrus clouds (High2/Low2). In general, high clouds and cirrus clouds are widespread, frequently covering the ITCZ, the tropical warm pool (from the western Pacific to the Indian Ocean), central Africa, South America, and midlatitude storm-track regions in both hemispheres. They are less frequent in subtropical oceans and from the Middle East to the Sahara. These distributions are similar to previous studies (e.g., Wylie et al. 1994; Jin et al. 1996), but differ-

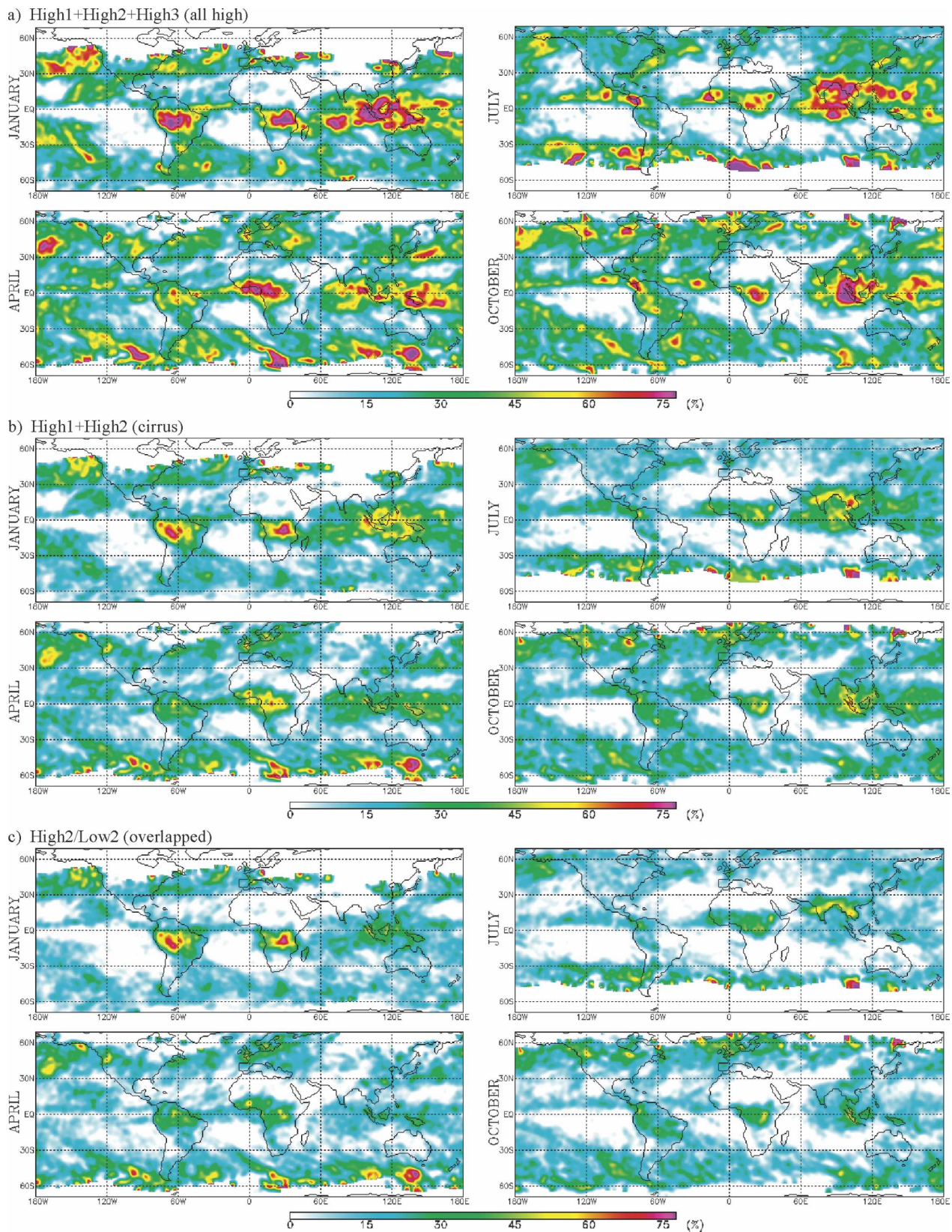


FIG. 9. Geographic distributions of monthly mean overcast high cloud ( $P_c < 500$  hPa) amounts for (a) all high clouds, (b) cirrus clouds, and (c) overlapped cirrus clouds in January, April, July, and October 2001.

ences do exist and are partly due to our 5-km overcast scene selections. For example, we have significantly less overcast high-cloud amounts between 30°S and 30°N than do the coarse-resolution HIRS data (maximum high-cloud amounts >70%). We also found less high clouds in July. In comparisons between Figs. 9a and 9b, large differences due to High3 clouds are found in regions with relatively large high-cloud amounts (red areas in the Tropics). This implies that deep convective clouds (High3) lead to more cirrus clouds (High1 + High2). However, cirrus clouds are not necessarily associated with High3 clouds because they have more extensive coverage (Fig. 9b). The overlapped cirrus clouds (Fig. 9c) account for nearly 50% of all high clouds. The overall near-global mean cloud amounts in January, April, July, and October of 2001 are 25%, 26%, 20%, and 25% for all high clouds; 17%, 19%, 13%, and 17% for cirrus clouds; and 13%, 14%, 10%, and 13% for overlapped cirrus clouds, respectively.

The distributions of monthly mean low-cloud ( $P_c > 500 \text{ hPa}$ ) amount are shown in Fig. 10a for single-layer low clouds (Low1 + Mid) and in Fig. 10b for single-layer plus overlapped low clouds (Low1 + Mid + Low2). A comparison between Figs. 10a and 10b reveals that, in the Tropics, cloud overlapping accounts for a large portion of the underlying Low2 clouds where cirrus clouds are most extensive. The near-global mean low-cloud amounts in January, April, July, and October of 2001 are 22%, 19%, 21%, and 20% for the single-layer clouds (Fig. 10a), respectively, which increases to 35%, 33%, 31%, and 33% after adding the overlapped Low2 clouds (Fig. 10b). To compare our results with the ISCCP data where middle clouds are defined for  $P_c$  between 440 and 680 hPa (Rossow and Schiffer 1999; Zhang et al. 2005), we recalculated our middle-cloud amounts accordingly as shown in Fig. 10c. Our new middle-level cloud amounts are less than 10% on a global average. This is much smaller than the middle-level cloud amounts (18%) obtained from the ISCCP data (Jin et al. 1996). The middle clouds, while in scattered places, are found more often in high latitudes than low latitudes. Larger ISCCP middle-cloud amounts are attributed to the mixed signals from overlapped cirrus and low clouds, which are treated as single-layer middle clouds (Chang and Li 2005).

#### 4. Comparisons with the MODIS standard products

In our retrievals,  $\tau_{\text{VIS}}$  for single-layered cirrus clouds (High1) and overlapped cirrus clouds (High2) are estimated using an infrared radiative transfer scheme. The MODIS standard product (MOD06) uses reflectance

measurements for cirrus  $\tau_{\text{VIS}}$  retrievals, which depends more on the choice of ice crystal scattering phase function. To investigate any differences in the two retrievals, Fig. 11 shows the latitudinal distributions of zonal-mean  $\tau_{\text{VIS}}$  obtained from the MODIS standard products for the cases corresponding to the cloud categories classified by our algorithm as shown in Fig. 8c. The monthly mean  $\tau_{\text{VIS}}$  for the MODIS products are given in Table 4. The two sets of  $\tau_{\text{VIS}}$  products (MODIS and ours) are very similar in terms of both means (cf. Tables 3 and 4) and standard deviations (not shown), except for large differences for the overlapped clouds (High2/Low2). One might think that the MODIS retrievals for these clouds would be equivalent to the sum of  $\tau_{\text{VIS}}$  for our High2 and Low2 clouds, but this is not the case. Our High2  $\tau_{\text{VIS}}$  was retrieved assuming ice cloud and our Low2  $\tau_{\text{VIS}}$  was retrieved assuming water cloud, but the MODIS High2\*  $\tau_{\text{VIS}}$  was retrieved assuming a single-column ice cloud. This leads to smaller MODIS High2\*  $\tau_{\text{VIS}}$  by an average of ~30% than the sum of our High2  $\tau_{\text{VIS}}$  and Low2  $\tau_{\text{VIS}}$  as shown in Table 3. However, if the MODIS High2\* were retrieved by assuming a total-water cloud, the MODIS  $\tau_{\text{VIS}}$  would be larger than the sum of High2 plus Low2  $\tau_{\text{VIS}}$ . So, for cirrus overlapping water clouds, a single-layer algorithm assuming ice or water cloud may be biased either way.

Figure 12 compares the zonal-mean High1  $\tau_{\text{VIS}}$  derived from our IR method and from the MODIS VIS reflectance method at  $0.86 \mu\text{m}$  over oceans (Fig. 12a) and  $0.65 \mu\text{m}$  over land (Fig. 12b). Each point represents a monthly zonal mean for each  $1^\circ$  latitudinal band. The MODIS VIS-retrieved cirrus  $\tau_{\text{VIS}}$  are on average larger by ~0.25 (a bit more over land) than our IR retrievals and the differences increase with increasing  $\tau_{\text{VIS}}$ . The differences may involve various uncertainties due to surface reflectance, choice of ice particle size and ice crystal scattering phase function, and  $\tau_{\text{IR}}$  to  $\tau_{\text{VIS}}$  conversion, etc. Note that MODIS also retrieves cloud effective radius  $r_e$  in addition to  $\tau_{\text{VIS}}$ , whereas  $r_e$  is fixed in our IR retrieval. The relationship given by Eq. (4), used for converting  $\tau_{\text{IR}}$  to  $\tau_{\text{VIS}}$ , is also uncertain. Because we do not find any systematic trend with respect to surface reflectance and  $r_e$ , the biased slope in Fig. 12 may imply that the  $\tau_{\text{IR}}$  to  $\tau_{\text{VIS}}$  conversion factor of  $\xi = 2.13$  is underestimated. To get results in agreement with the MODIS product, we could modify the ratio factor to  $\xi = 2.52$  for over ocean and  $\xi = 2.56$  for over land, but this modification lacks a physical basis.

The MODIS High3  $\tau_{\text{VIS}}$  shown in Table 4 are also larger than our High3  $\tau_{\text{VIS}}$  shown in Table 3. This is probably because all our High3 clouds were considered ice clouds but some of these High3 clouds were retrieved as water clouds by MODIS. The water-cloud

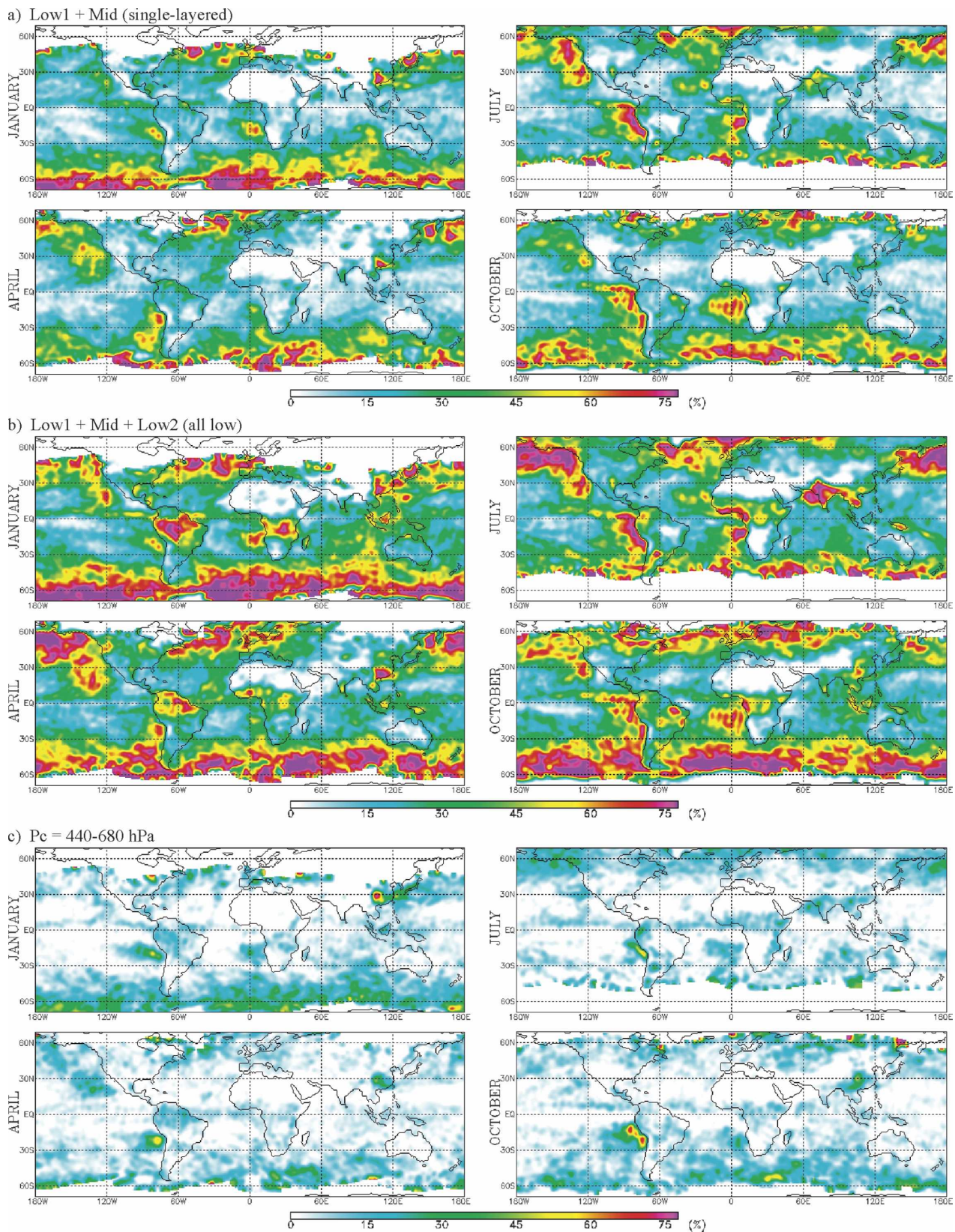


FIG. 10. Geographic distributions of monthly mean overcast low cloud ( $P_c \geq 500 \text{ hPa}$ ) amounts for (a) Low1 + Mid, (b) Low1 + Mid + Low2, and (c) middle-level clouds ( $P_c = 440-680 \text{ hPa}$ ) in January, April, July, and October 2001.

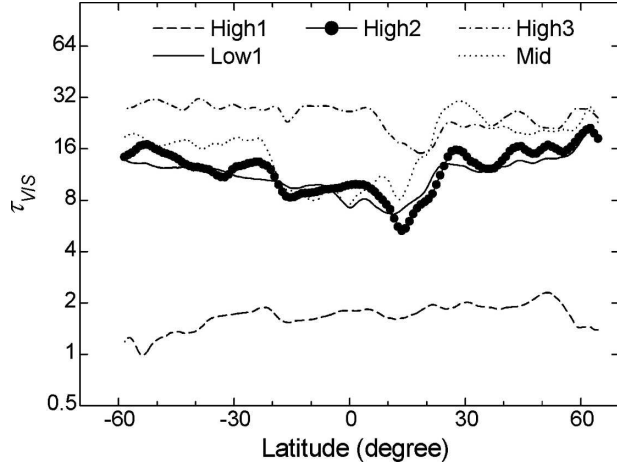


FIG. 11. Latitudinal variations of zonal-mean  $\tau_{\text{VIS}}$  from the MODIS standard products but corresponding to High1, High2\*, High3, Mid, and Low1 classified by our algorithm in April 2001.

model usually leads to a larger  $\tau_{\text{VIS}}$  retrieval than the ice cloud model (Rossow and Schiffer 1999). For lower clouds dominated by water drops, the two retrievals agree well. The zonal-mean  $\tau_{\text{VIS}}$  for single-layer cirrus clouds also shows a good agreement between the two retrievals (within 5%). These results corroborate our assumption of using a constant  $r_e$  for water (10  $\mu\text{m}$ ) and ice (30  $\mu\text{m}$ ) clouds.

Figure 13 shows the latitudinal distributions of MODIS zonal-mean  $\varepsilon_{\text{hc}}$  (April 2001 only) corresponding to our classification of High1, High2, and High3 clouds. The MODIS  $\varepsilon_{\text{hc}}$  and ours are identical for High1 and High3 clouds, but different for High2 clouds. The  $\varepsilon_{\text{hc}}$  from our retrievals (line with open circles, High2) were obtained using Eq. (5) whereas those from the MODIS standard products (line with solid circles, High2\*) were derived from Eq. (1) assuming no low clouds. Similar results can be seen by comparing the global mean  $\varepsilon_{\text{hc}}$  for all months given in Table 3 for High1, High2, and High3 clouds and in Table 4 for High2\*  $\varepsilon_{\text{hc}}$ . If there is no correction to account for the

TABLE 4. As in Table 3, but for MODIS standard products  $\tau_{\text{VIS}}$  for High1, High2\*, High3, Mid, and Low1 and  $\varepsilon_{\text{hc}}$  for High2\*.

	Jan 2001	Apr 2001	Jul 2001	Oct 2001	Mean
$\tau_{\text{VIS}}$					
High1	1.69/1.65	1.65/1.73	1.77/1.89	1.65/1.73	1.69/1.75
High2*	12.5/10.8	12.3/11.9	12.6/13.2	12.8/11.9	12.6/12.0
High3	25.9/24.8	25.4/24.5	27.1/27.4	26.9/25.3	26.3/25.5
Mid	16.1/13.5	16.8/15.4	17.1/16.5	18.0/15.0	17.0/15.1
Low1	11.2/10.5	11.0/11.1	10.8/11.4	11.3/10.9	11.1/11.0
$\varepsilon_{\text{hc}}$					
High2*	0.64/0.61	0.61/0.60	0.64/0.65	0.64/0.62	0.63/0.62

\* MODIS standard single-layer retrieval.

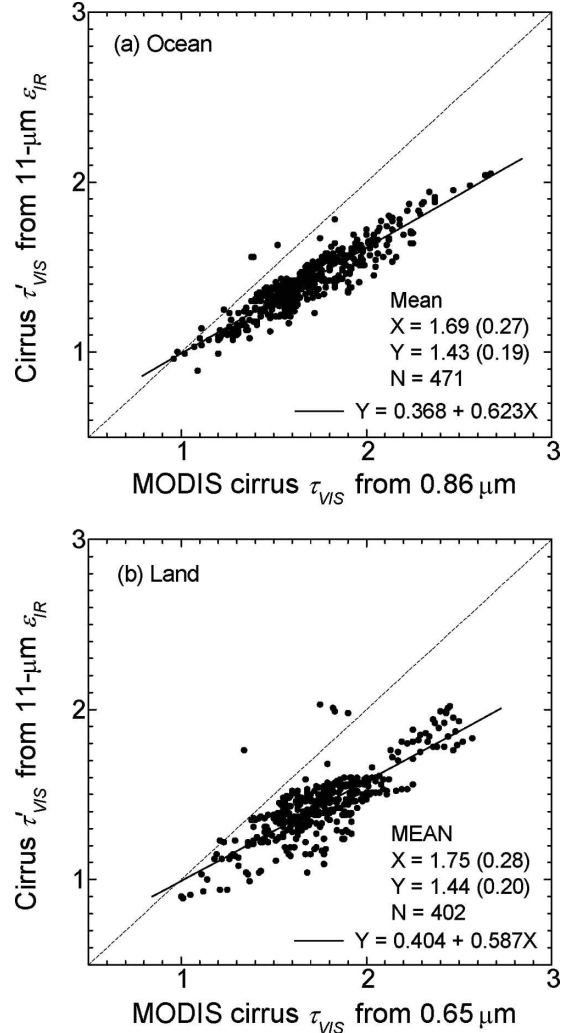


FIG. 12. Comparisons of 1° zonal monthly mean cirrus cloud optical depths from our retrieval and the operational MODIS retrieval at (a) 0.86  $\mu\text{m}$  over ocean and (b) 0.65  $\mu\text{m}$  over land in January, April, July, and October 2001. The overall means (standard deviations), total number of samples, and least squares fitting are given in each subplot.

overlapping effect of the low clouds,  $\varepsilon_{\text{hc}}$  can be overestimated by a mean bias of  $\Delta\varepsilon_{\text{hc}} \sim 0.10$ .

Since the MODIS CO<sub>2</sub>-slicing technique assumes a single-layer cloud, the MODIS products of  $P_c$  and  $T_c$  for the overlapped High2 clouds are probably also biased. In reference to Table 3, they seem to be overestimated by a mean bias of  $\Delta P_c \sim 38$  hPa and  $\Delta T_c \sim 7$  K when compared with the  $P_c$  and  $T_c$  of High1 clouds. For the data analyzed in this study, we have not modified the MODIS  $T_c$  (or  $P_c$ ). However, if the High2 cirrus  $T_c$  are decreased by 7 K (from 236 to 229 K), our High2  $\varepsilon_{\text{hc}}$  according to Eq. (5) would only decrease by about 0.01–0.02 on a monthly mean basis. Such effects would also be small on the retrieved cirrus  $\tau_{\text{VIS}}$  and

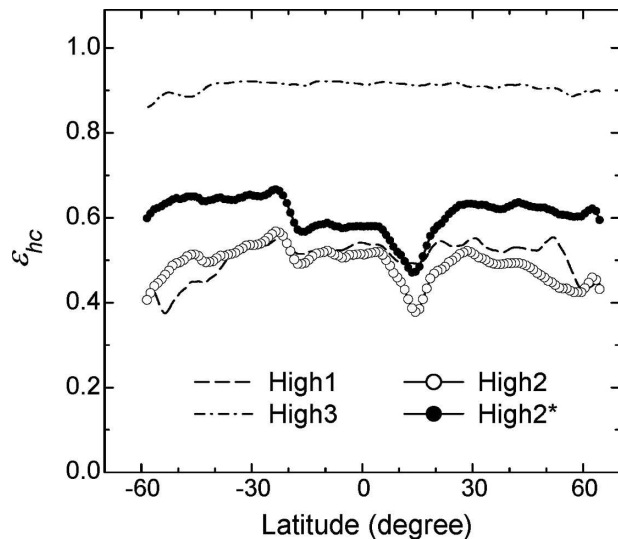


FIG. 13. Latitudinal variations of the zonal-mean high-cloud emissivity according to our classifications of High1, High2, and High3, and High2\* (MODIS product) in April 2001.

their overlapped low-cloud  $\tau_{\text{VIS}}$ . Errors associated with the MODIS CO<sub>2</sub>-slicing Pc/Tc should have little impact on our analyses of overlapped cirrus cloud amounts and differentiated  $\tau_{\text{VIS}}$  retrievals for the overlapped cirrus and low clouds.

As a first-order approximation to correct for the potential Pc biases in overlapped cirrus clouds, we propose an empirical formula,

$$\frac{\Delta \text{Pc}}{\Delta \varepsilon_{\text{hc}}} = \frac{(\text{Pc} - \text{Pc}^*)}{(\varepsilon_{\text{hc}} - \varepsilon_{\text{hc}}^*)}, \quad (6)$$

where  $\text{Pc}^*$  and  $\varepsilon_{\text{hc}}^*$  denote the biased values from the MODIS products,  $\varepsilon_{\text{hc}}$  denotes the value from our retrieval, and  $\Delta \text{Pc}$  (38 hPa) and  $\Delta \varepsilon_{\text{hc}}$  (0.10) denote the mean biases obtained in this study. The corrected Pc and Tc can thus be obtained from the following expressions:

$$\text{Pc} = \text{Pc}^* + (\Delta \text{Pc} / \Delta \varepsilon_{\text{hc}})(\varepsilon_{\text{hc}} - \varepsilon_{\text{hc}}^*), \quad (7)$$

$$\text{Tc} = \text{Tc}^* + (\Delta \text{Tc} / \Delta \varepsilon_{\text{hc}})(\varepsilon_{\text{hc}} - \varepsilon_{\text{hc}}^*). \quad (8)$$

From Eqs. (7)–(8), our revised High2  $\tau_{\text{VIS}}$  decreases by  $\sim 0.1$  on a monthly mean basis. This indeed brings our High2 mean  $\tau_{\text{VIS}}$  closer to our High1 mean  $\tau_{\text{VIS}}$ , as revealed in Table 3. Our Low2 mean  $\tau_{\text{VIS}}$  increases by a similar magnitude ( $\sim 0.1$ ), which is negligible relative to  $\tau_{\text{VIS}} \sim 12\text{--}14$ .

## 5. Concluding remarks

The global distribution of cloud vertical structure is crucial for climate studies due to its impact on both the magnitude and sign of the net cloud–radiative forcing

and the adiabatic heating profile of the atmosphere. So far, we have very poor knowledge of cloud vertical distribution on a global scale due to limited spectral channel information, essentially one visible channel and one infrared channel. These two spectral channels may provide bulk information for single-layer clouds but cannot resolve the vertical distribution in any detail, especially for semitransparent cirrus overlapping low clouds.

The significantly advanced MODIS instrument provides much richer information, but the current standard MODIS cloud algorithms employ a single-layer cloud model that cannot separate overlapped cirrus and low clouds. To overcome this limitation, a novel retrieval method is employed that can differentiate single-layer and overlapped cirrus clouds and retrieve their individual optical properties. The method was applied to near-global (polar regions excluded) MODIS data acquired in January, April, July, and October of 2001. The data were sampled one out of every four days. Calibrated radiance data from the MODIS Level-1B 1-km aggregated product were processed and the analyses are limited to 5-km overcast scenes, which account for approximately 75% of the total MODIS cloud coverage ( $\sim 0.60$ ). We classified clouds into six categories: single-layer and overlapped cirrus clouds, single-layer and overlapped low clouds, optically thick high clouds, and midlevel clouds. Their individual frequency of occurrence, cloud-top pressure/temperature (Pc/Tc), optical depth ( $\tau_{\text{VIS}}$ ), and high-cloud emissivity ( $\varepsilon_{\text{hc}}$ ) are derived.

Of all 5-km overcast scenes that are analyzed over oceans and land (in parentheses): 52% (61%) are high clouds with  $\text{Pc} < 500$  hPa and 48% (39%) are lower clouds with  $\text{Pc} > 500$  hPa. There are less than 10% of middle level clouds with  $\text{Pc}$  falling between 440 and 680 hPa and fewer than 4% between 500 and 600 hPa. The data also contain 35% (41%) cirrus clouds ( $\varepsilon < 0.85$  and  $\text{Pc} < 500$  hPa) and 27% (29%) cirrus overlapping lower clouds. After accounting for the overlapped low clouds, the percentages of low clouds increase to 75% (48% + 27%) over oceans and 68% (39% + 29%) over land. The retrieved cirrus clouds have a mean value of  $\tau_{\text{VIS}} \sim 1.5$  and  $\varepsilon_{\text{hc}} \sim 0.5$ , which are very similar for both single-layer and overlapped cirrus clouds.

For the majority of clouds, their tops tend to be located somewhere within two distinct layers in the upper and lower troposphere; the cloud-top pressures in these two layers peak at 275 and 725 hPa. There is a distinct minimum  $\text{Pc}$  occurrence between 500 and 600 hPa, a ubiquitous phenomenon occurring at almost all latitudes and in all seasons. This characteristic may shed light on understanding cloud dynamical and radiative

processes for improving cloud and climate modeling. Note that this phenomenon does not result from the use of our two-layer retrieval model because the model can identify and retrieve both single- and two-layered clouds at any altitude. However, this and any other method could miss multilayer clouds below thick high clouds.

MODIS products only provide the highest cloud top for both single-layer and overlapped clouds, so use of these cloud-top data would underestimate low clouds by about 30% if there were cirrus overlapping. The optical depths of overlapped cirrus clouds would be overestimated by a factor of about 7 due to the optically thicker water clouds underneath. In comparison, ISCCP has much more middle cloud and less high and low clouds and thus does not show a distinct two-layer cloud structure due to a fundamental limit of IR measurements in differentiating overlapped high and low clouds from single-layer middle clouds. The HIRS data have much more high and middle clouds, but their coarse spatial resolution ( $\sim 20$  km) gives large uncertainties.

In light of the substantial differences in cloud vertical structure, much caution is warranted in both validating general circulation models (GCMs) and improving their cloud parameterization schemes. At present, results of cloud simulations from many GCMs have been validated against ISCCP total cloud amounts, resulting in many improvements in the models. More attention is now being paid to more detailed comparisons concerning the vertical distribution of clouds, or clouds occurring in different layers. For example, the current ARM Cloud Parameterization and Modeling (ARMCPM) working group has collected and analyzed 10 sets of GCM-simulated cloud-layer data and compared them to the statistics of the ISCCP data (Zhang et al. 2005). It was found that most GCMs produce substantially less middle and low clouds than the ISCCP. In general, compared to that of the ISCCP, the GCM middle level cloud amounts are closer to our new retrieval products, whereas the GCM low-cloud amounts are quite different from our retrievals. Clearly, it is critical to sort out these differences in order to improve the performance of GCMs and other types of models of higher resolution.

**Acknowledgments.** This research would not have been possible without the dedicated work of the MODIS Atmospheres Team in processing the cloud mask and cloud properties. The authors are grateful to the NASA Goddard Earth Sciences (GES) Distributed Active Archived Center (DAAC) for providing the MODIS data. Funding for this work was supported by

DOE Grant DE-FG02-01ER63166 under the ARM program and NASA Grant NNG04GE79G.

## REFERENCES

- Ackerman, S. A., K. I. Strabala, W. P. Menzel, R. A. Frey, C. C. Moeller, and L. E. Gumley, 1998: Discriminating clear-sky from clouds with MODIS. *J. Geophys. Res.*, **103**, 32 141–32 158.
- Agee, E. M., 1984: Observations from space and thermal convection: A historical perspective. *Bull. Amer. Meteor. Soc.*, **65**, 938–949.
- Armstrong, R. L., and M. J. Brodzik, 2001: Recent northern hemisphere snow extent: A comparison of data derived from visible and microwave satellite sensors. *Geophys. Res. Lett.*, **28**, 3673–3676.
- Barnes, W. L., T. S. Pagano, and V. V. Salomonson, 1998: Pre-launch characteristics of the Moderate Resolution Imaging Spectroradiometer (MODIS) on EOS-AM1. *IEEE Trans. Geosci. Remote Sens.*, **36**, 1088–1100.
- Baum, B. A., and B. A. Wielicki, 1994: Cirrus cloud retrieval using infrared sounding data: Multilevel cloud errors. *J. Appl. Meteor.*, **33**, 107–117.
- , and J. D. Spinhirne, 2000: Remote Sensing of cloud properties using MODIS airborne simulator imagery during SUCCESS. 3. Cloud overlap. *J. Geophys. Res.*, **105**, 11 793–11 804.
- , and Coauthors, 1995: Satellite remote sensing of multiple cloud layers. *J. Atmos. Sci.*, **52**, 4210–4230.
- , V. Tovinkere, J. Titlow, and R. M. Welch, 1997: Automated cloud classification of global AVHRR data using a fuzzy logic approach. *J. Appl. Meteor.*, **36**, 1519–1540.
- Berk, A., and Coauthors, 1999: MODTRAN4 v. 2.0 user's manual. Air Force Geophysics Laboratory Tech. Rep. AFGL-TR-89-0122, 98 pp.
- Chang, F.-L., and Z. Li, 2002: Estimating the vertical variation of cloud droplet effective radius using multispectral near-infrared satellite measurements. *J. Geophys. Res.*, **107**, 4257, doi:10.1029/2001JD000766.
- , and —, 2005: A new method for detection of cirrus overlapping water clouds and determination of their optical properties. *J. Atmos. Sci.*, **62**, 3993–4009.
- Clothiaux, E. E., T. P. Ackerman, G. G. Mace, K. P. Moran, R. T. Marchand, M. Miller, and B. E. Martner, 2000: Objective determination of cloud heights and radar reflectivities using a combination of active remote sensors at the ARM CART Sites. *J. Appl. Meteor.*, **39**, 645–665.
- COESA, 1976: *U.S. Standard Atmosphere, 1976*. U.S. Government Printing Office, 227 pp.
- Comstock, J. M., and K. Sassen, 2001: Retrieval of cirrus cloud radiative and backscattering properties using combined lidar and infrared radiometer (LIRAD) measurements. *J. Atmos. Oceanic Technol.*, **18**, 1658–1673.
- , and C. Jakob, 2004: Evaluation of tropical cirrus cloud properties derived from ECMWF model output and ground based measurements over Nauru Island. *Geophys. Res. Lett.*, **31**, L10106, doi:10.1029/2004GL019539.
- Derber, J. C., D. F. Parrish, and S. J. Lord, 1991: The new global operational analysis system at the National Meteorological Center. *Wea. Forecasting*, **6**, 538–547.
- Descloitres, J. C., J. C. Buriez, F. Parol, and Y. Fouquart, 1998: POLDER observations of cloud bidirectional reflectances compared to a plane-parallel model using the International

- Satellite Cloud Climatology Project cloud phase functions. *J. Geophys. Res.*, **103**, 11 411–11 418.
- Francis, P. N., 1995: Some aircraft observations of the scattering properties of ice crystals. *J. Atmos. Sci.*, **52**, 1142–1154.
- Hale, G. M., and M. R. Quarry, 1973: Optical constants of water in the 200 nm to 200 mm wavelength region. *Appl. Opt.*, **12**, 555–563.
- Hartmann, D. L., M. E. Ockert-Bell, and M. L. Michelsen, 1992: The effect of cloud type on Earth's energy balance: Global analysis. *J. Climate*, **5**, 1281–1304.
- Ho, S.-P., B. Lin, P. Minnis, and T.-F. Fan, 2003: Estimates of cloud vertical structure and water amount over tropical oceans using VIRS and TMI data. *J. Geophys. Res.*, **108**, 4419, doi:10.1029/2002JD003298.
- Jacobowitz, H., L. L. Stowe, G. Ohring, A. Heidinger, K. Knapp, and N. R. Nalli, 2003: The Advanced Very High Resolution Radiometer Pathfinder Atmosphere (PATMOS) climate dataset: A resource for climate research. *Bull. Amer. Meteor. Soc.*, **84**, 785–793.
- Jin, Y., W. B. Rossow, and D. P. Wylie, 1996: Comparison of the climatologies of high-level clouds from HIRS and ISCCP. *J. Climate*, **9**, 2850–2879.
- Johnson, R. H., T. M. Rickenbach, S. A. Rutledge, P. E. Ciesielski, and W. H. Schubert, 1999: Trimodal characteristics of tropical convection. *J. Climate*, **12**, 2397–2418.
- King, M. D., and Coauthors, 2003: Cloud and aerosol properties, precipitable water, and profiles of temperature and humidity from MODIS. *IEEE Trans. Geosci. Remote Sens.*, **41**, 442–458.
- Kuettner, J. P., 1971: Cloud bands in the earth's atmosphere. *Tellus*, **23**, 404–425.
- Lin, B., P. Minnis, B. Wielicki, D. R. Doelling, R. Palikonda, D. F. Young, and T. Uttal, 1998: Estimation of water cloud properties from satellite microwave, infrared and visible measurements in oceanic environment: 2. Results. *J. Geophys. Res.*, **103**, 3887–3905.
- Liou, K. N., 1986: Influence of cirrus clouds on weather and climate processes: A global perspective. *Mon. Wea. Rev.*, **114**, 1167–1199.
- Liu, C., and M. W. Moncrieff, 1998: A numerical study of the diurnal cycle of tropical oceanic convection. *J. Atmos. Sci.*, **55**, 2329–2344.
- Mace, G. G., and S. Benson-Troth, 2002: Cloud-layer overlap characteristics derived from long-term cloud radar data. *J. Climate*, **15**, 2505–2515.
- , E. E. Clothiaux, and T. A. Ackerman, 2001: The composite characteristics of cirrus clouds: Bulk properties revealed by one year of continuous cloud radar data. *J. Climate*, **14**, 2185–2203.
- Macke, A., 1993: Scattering of light by polyhedral ice crystals. *Appl. Opt.*, **32**, 2780–2788.
- Menzel, W. P., D. P. Wylie, and K. I. Strabala, 1992: Seasonal and diurnal changes in cirrus clouds as seen in four years of observations with the VAS. *J. Appl. Meteor.*, **31**, 370–385.
- , B. A. Baum, K. I. Strabala, and R. A. Frey, 2002: Cloud top properties and cloud phase—Algorithm Theoretical Basis Doc. ATBD-MOD-04, 61 pp. [Available online at [http://modis-atmos.gsfc.nasa.gov/\\_docs/atbd\\_mod04.pdf](http://modis-atmos.gsfc.nasa.gov/_docs/atbd_mod04.pdf).]
- Minnis, P., D. F. Young, K. Sassen, J. M. Alvarez, and C. J. Grund, 1990: The 27–28 October 1986 FIRE IFO cirrus case study: Cirrus parameter relationships derived from satellite and lidar data. *Mon. Wea. Rev.*, **118**, 2402–2425.
- , K.-N. Liou, and Y. Takano, 1993a: Inference of cirrus cloud properties using satellite-observed visible and infrared radiances. Part I: Parameterization of radiance field. *J. Atmos. Sci.*, **50**, 1279–1304.
- , P. W. Heck, and D. F. Young, 1993b: Inference of cirrus cloud properties using satellite-observed visible and infrared radiances. Part II: Verification of theoretical cirrus radiative properties. *J. Atmos. Sci.*, **50**, 1305–1322.
- Mishchenko, M. I., W. B. Rossow, A. Macke, and A. A. Lacis, 1996: Sensitivity of cirrus cloud albedo, bidirectional reflectance, and optical thickness retrieval accuracy to ice-particle shape. *J. Geophys. Res.*, **101**, 16 973–16 985.
- Ou, S. C., K. N. Liou, and B. A. Baum, 1996: Detection of multi-layer cirrus cloud systems using AVHRR data: Verification based on FIRE-II IFO composite measurements. *J. Appl. Meteor.*, **35**, 178–191.
- Pincus, R., S. A. McFarlane, and S. A. Klein, 1999: Albedo bias and the horizontal variability of clouds in subtropical marine boundary layers: Observations from ships and satellites. *J. Geophys. Res.*, **104**, 6183–6191.
- Pavolonis, M. J., and A. K. Heidinger, 2004: Daytime cloud overlap detection from AVHRR and VIIRS. *J. Appl. Meteor.*, **43**, 762–778.
- Platnick, S., M. D. King, S. A. Ackerman, W. P. Menzel, B. A. Baum, J. C. Riedi, and R. A. Frey, 2003: The MODIS cloud products: Algorithms and examples from *Terra*. *IEEE Trans. Geosci. Remote Sens.*, **41**, 459–473.
- Platt, C. M. R., and G. L. Stephens, 1980: The interpretation of remotely sensed high cloud emittances. *J. Atmos. Sci.*, **37**, 2314–2322.
- , and Coauthors, 1994: The Experimental Cloud Lidar Pilot Study (ECLIPS) for cloud–radiation research. *Bull. Amer. Meteor. Soc.*, **75**, 1635–1654.
- Poore, K., J. Wang, and W. B. Rossow, 1995: Cloud layer thicknesses from a combination of surface and upper-air observations. *J. Climate*, **8**, 550–568.
- Ramaswamy, V., and V. Ramanathan, 1989: Solar absorption by cirrus clouds and the maintenance of the tropical upper troposphere thermal structure. *J. Atmos. Sci.*, **46**, 2293–2310.
- Randall, D. A., Harshvardhan, D. A. Dazlich, and T. G. Gorsetti, 1989: Interactions among radiation, convection, and large-scale dynamics in a general circulation model. *J. Atmos. Sci.*, **46**, 1943–1970.
- Rossow, W. B., and R. A. Schiffer, 1991: ISCCP cloud data products. *Bull. Amer. Meteor. Soc.*, **72**, 2–20.
- , and —, 1999: Advances in understanding clouds from ISCCP. *Bull. Amer. Meteor. Soc.*, **80**, 2261–2287.
- , L. C. Garder, and A. A. Lacis, 1989: Global, seasonal cloud variations from satellite radiance measurements. Part I: Sensitivity of analysis. *J. Climate*, **2**, 419–462.
- Sassen, K., 1991: The polarization lidar technique for cloud research: A review and current assessment. *Bull. Amer. Meteor. Soc.*, **72**, 1848–1866.
- , Z. Wang, C. M. R. Platt, and J. M. Comstock, 2003: Parameterization of infrared absorption in midlatitude cirrus clouds. *J. Atmos. Sci.*, **60**, 428–433.
- Sherwood, S. C., V. Ramanathan, T. P. Barnett, M. K. Tyree, and E. Roeckner, 1994: Response of an atmospheric general circulation model to radiative forcing of tropical clouds. *J. Geophys. Res.*, **99**, 20 829–20 845.
- Sheu, R.-S., J. A. Curry, and G. Liu, 1997: Vertical stratification of tropical cloud properties as determined from satellite. *J. Geophys. Res.*, **102**, 4231–4245.
- Starr, D. O'C., and S. K. Cox, 1985: Cirrus clouds. Part II: Nu-

- merical experiments on the formation and maintenance of cirrus. *J. Atmos. Sci.*, **42**, 2682–2694.
- Stephens, G. L., S.-C. Tsay, P. W. Stackhouse Jr., and P. J. Flatau, 1990: The relevance of the microphysical and radiative properties of cirrus clouds to climate and climate feedbacks. *J. Atmos. Sci.*, **47**, 1742–1753.
- , and Coauthors, 2002: The CLOUDSAT mission and the A-Train: A new dimension of space-based observations of clouds and precipitation. *Bull. Amer. Meteor. Soc.*, **83**, 1771–1790.
- Stowe, L. L., H. Jacobowitz, G. Ohring, K. R. Knapp, and N. R. Nalli, 2002: The Advanced Very High Resolution Radiometer (AVHRR) Pathfinder Atmosphere (PATMOS) climate dataset: Initial analyses and evaluations. *J. Climate*, **15**, 1243–1260.
- Takano, Y., and K.-N. Liou, 1989: Solar radiative transfer in cirrus clouds. Part I: Single scattering and optical properties of hexagonal ice crystal. *J. Atmos. Sci.*, **46**, 3–19.
- Tselioudis, G., W. B. Rossow, and D. Rind, 1992: Global patterns of cloud optical thickness variation with temperature. *J. Climate*, **5**, 1484–1495.
- Wang, J., W. B. Rossow, and Y. Zhang, 2000: Cloud vertical structure and its variations from a 20-yr global rawinsonde dataset. *J. Climate*, **13**, 3034–3056.
- Warren, S. G., 1984: Optical constants of ice from ultraviolet to the microwave. *Appl. Opt.*, **23**, 1206–1225.
- , C. J. Hahn, and J. London, 1985: Simultaneous occurrence of different cloud types. *J. Climate Appl. Meteor.*, **24**, 658–667.
- Wielicki, B. A., and L. Parker, 1992: On the determination of cloud cover from satellite sensors: The effect of sensor spatial resolution. *J. Geophys. Res.*, **97**, 12 799–12 823.
- Wylie, D. P., and W. P. Menzel, 1989: Two years of cloud cover statistics using VAS. *J. Climate*, **2**, 380–392.
- , —, 1999: Eight years of high cloud statistics using HIRS. *J. Climate*, **12**, 170–184.
- , —, H. M. Woolf, and K. I. Strabala, 1994: Four years of global cirrus cloud statistics using HIRS. *J. Climate*, **7**, 1972–1986.
- Zhang, M. H., and Coauthors, 2005: Comparing clouds and their seasonal variations in 10 atmospheric general circulation models with satellite measurements. *J. Geophys. Res.*, **110**, D15S02, doi:10.1029/2005JD005021.
- Zuidema, P., 1998: The 600–800-mb minimum in tropical cloudiness observed during TOGA COARE. *J. Atmos. Sci.*, **55**, 2220–2228.